LEVEL II (3)

Progress Report on the Study of the Fundamental Mechanisms
of Unconfined Detonation of Fuel-Air Explosions
for the period Jan. 1, 1979 to Dec. 31, 1980

ADA084367

Submitted by

Dr. R. Knystautas
Dr. J.H. Lee
Dr. I.O. Moen

McGill University
Montreal, Canada

February 1980

AFOSR-77-3207

80 5 14 098

DISCLAIMER NOTICE

THIS DOCUMENT IS BEST QUALITY
PRACTICABLE. THE COPY FURNISHED
TO DTIC CONTAINED A SIGNIFICANT
NUMBER OF PAGES WHICH DO NOT
REPRODUCE LEGIBLY.

REPORT DOCUMENTATION PAGE	READ INSTRUCTIONS BEFORE COMPLETING FORM

1. REPORT NUMBER AFOSR-TR- 80 - 0323	2. GOVT ACCESSION NO. AD-A094367	3. RECIPIENT'S CATALOG NUMBER

4. TITLE (and Subtitle) FUNDAMENTAL MECHANISMS OF UNCONFINED DETONATION OF FUEL-AIR EXPLOSIONS	5. TYPE OF REPORT & PERIOD COVERED INTERIM Jan. 1, 1979 - Dec. 31, 1979
	6. PERFORMING ORG. REPORT NUMBER

7. AUTHOR(s) R. Knystautas, J.H. Lee, I.O. Moen	8. CONTRACT OR GRANT NUMBER(s) AFOSR-77-3207

9. PERFORMING ORGANIZATION NAME AND ADDRESS MCGILL UNIVERISTY DEPARTMENT OF MECHANICAL ENGINEERING 817 SHERBROOKE ST WEST/MONTREAL, PQ, CANADA H3A 2K6	10. PROGRAM ELEMENT, PROJECT, TASK AREA & WORK UNIT NUMBERS 2308/A2 61102F

11. CONTROLLING OFFICE NAME AND ADDRESS AIR FORCE OFFICE OF SCIENTIFIC RESEARCH/NA BLDG 410 BOLLING AIR FORCE BASE, D C 20332	12. REPORT DATE Feb 80
	13. NUMBER OF PAGES 97

14. MONITORING AGENCY NAME & ADDRESS(if different from Controlling Office)	15. SECURITY CLASS. (of this report) UNCLASSIFIED
	15a. DECLASSIFICATION/DOWNGRADING SCHEDULE

16. DISTRIBUTION STATEMENT (of this Report)

Approved for public release; distribution unlimited.

17. DISTRIBUTION STATEMENT (of the abstract entered in Block 20, if different from Report)

18. SUPPLEMENTARY NOTES

19. KEY WORDS (Continue on reverse side if necessary and identify by block number)

Fuel-Air Explosions
Explosion
Detonation
The FAE III Concept

Chemical Initiation
Volumetric Initiation
Chemical Kinetics
Turbulent Flame Propagation

Detonability Limits

20. ABSTRACT (Continue on reverse side if necessary and identify by block number)

Research during the past year has led to some significant results which have profound implications in the area of vapor cloud explosion in general, and in the area of "shockless" initiation of detonation in particular. In brief we have; i) demonstrated experimentally that initiation of detonation can be achieved by injecting a chemical catalyst into a fuel-air mixture, ii) demonstrated experimentally that direct initiation can be achieved by seeding

Cont'd. on reverse side...

DD FORM 1473

80 5 14 098

*Cont'd.

an explosive mixture with free radicals of the appropriate concentration and spatial distribution, iii) demonstrated experimentally that direct initiation can be achieved via turbulent mixing between an explosive mixture and its combustion products, iv) demonstrated experimentally that unconfined turbulent flame speeds exceeding 400 m/s can readily be achieved in a mixture as inert as methane air, v) clarified through experiments the role of confinement on the propagation of detonations near the detonability limits, and vi) assessed the far field destructive potential of FAE weapons by calculating numerically the effective blast energy of non-ideal blast waves generated by vapor cloud explosions.

Summary of Progress

Our recent studies have led to some significant results which have profound implications in the area of vapor cloud explosion in general, and in the area of "shockless" initiation of detonation in particular. In brief we have; i) demonstrated experimentally that initiation of detonation can be achieved by injecting a chemical catalyst into a fuel-air mixture, ii) demonstrated experimentally that direct initiation can be achieved by seeding an explosive mixture with free radicals of the appropriate concentration and spatial distribution, iii) demonstrated experimentally that direct initiation can be achieved via turbulent mixing between an explosive mixture and its combustion products, iv) demonstrated experimentally that unconfined turbulent flame speeds exceeding 400 m/s can readily be achieved in a mixture as inert as methane air, v) clarified through experiments the role of confinement on the propagation of detonations near the detonability limits, and vi) assessed the far field destructive potential of FAE weapons by calculating numerically the effective blast energy of non-ideal blast waves generated by vapor cloud explosions.

During the past year a significant milestone towards the realization of an FAE III device has been reached at McGill in that detonation in a premixed fuel-air system (propane-air) solely by injecting a chemical agent (fluorine) has been achieved on a laboratory scale. Laboratory scale experiments are of necessity small scale and confined, and a considerable research effort has been made to identify the fundamental underlying mechanisms and to establish quantitative criteria for the scaling up of these experiments in preparation for large scale bag tests to be performed at Eglin Air Force Base. A review of the progress in the area of Pyrophoric Initiation of Detonation in Fuel-Air Mixtures including a discussion of

criteria for scale-up and removal of confinement, as well as a discussion of the dispersion and mixing requirements are given in Appendix I.

The role of both large and small scale turbulence in augmenting the explosion of a fuel-air cloud have been further clarified by our investigations of turbulent flame propagation and acceleration in the presence of obstacles. These investigations have established that extremely high flame speeds and large overpressures can be obtained through the generation of large scale turbulent eddies and small scale turbulence in the unburned gas by placing repeated obstacles in the flame path. Laboratory scale experiments on unconfined cylindrically expanding methane-air flames with repeated obstacles in the flame path using both streak and schlieren diagnostic observations, together with larger scale experiments performed in collaboration with Professor Wagner at the University of Göttingen, have demonstrated that flame speeds in excess of 400 m/s with associated overpressures of the order of 0.65 bar can be generated in an obstacle environment. A simple theoretical model of the flame acceleration process based on a positive feedback mechanism between the flow field generated by the flame propagation over obstacles, and the burn-out of the large turbulent eddies predicts an exponential increase in flame velocity which is in good agreement with the experimental results. The current status of our investigations on turbulent flame propagation including detailed discussions of experimental and theoretical results is given in Appendix II.

The detonability limits determine the conditions beyond which an explosive mixture can no longer support a detonation. At the present time it is not possible to predict the detonability limits of a given mixture theoretically and the limits must be determined experimentally. Experiments to determine these limits are usually performed in detonation tubes, however the influence of confinement and the initiation source on the propagation

of detonations is not understood. Our investigation of the propagation of detonations in long tubes (14 m) of diameter 4.8 cm and 14.5 cm near the lean limit of detonability for ethylene-air at 1 atm shows that the propagation of marginal detonations are strongly influenced by both the initial conditions and the boundary conditions. In fact, completely different phenomena are observed for the same mixture composition depending on the initial and boundary conditions. Transverse spinning waves with wavelengths characteristic of the tube rather than the mixture are found to play a dominant role in the propagation of near-limit detonation waves. Because of this strong influence of the confinement a criteria for characterizing the detonability limits for unconfined detonations based on the onset of a single head spin has been proposed. Associated with this limit there is then a characteristic length equal to the tube diameter (or spin pitch), and by extrapolating from results in various diameter tubes the limit for unconfined detonations in a cloud of given size can be determined once the minimum number of transverse waves required for unconfined detonation is determined. A detailed discussion of the Influence of Confinement on the Propagation of Detonations near the Detonability Limits based on our results is given in Appendix III.

The far field destructive potential of fuel-air explosive weapons has been assessed by calculating numerically the effective blast energy of the non-ideal blast waves generated by vapor cloud explosives. For hydrocarbon-air and oxygen explosives, the effective blast energies represent approximately 37 and 27% of the respective combustion energy of the mixture, irrespective of the mode of combustion (i.e., detonation or volumetric explosion). Based on the effective blast energy, far field equivalence of non-ideal blast waves from fuel-air and oxygen explosives is demonstrated. In other words, the far field, non-ideal blast parameters (i.e., overpressure,

static and dynamic impulses) scale according to the explosion length based
on the effective blast energy and can be radily calculated from a single
chart to assess the destructive potential of fuel-air and oxygen explosive
weapons. Although all ideal point blast waves from solid explosive weapons
are equivalent and the corresponding blast parameters scale according to
the explosion length based on the total combustion energy of the charge, the
present study indicates that ideal and non-ideal blast waves are not equiva-
lent in the far field. In other words, at the same scaled distance, far
field blast parameters from ideal and non-ideal blast waves are no equal.
Based on the matching of the overpressure curves in the far field, the equi-
valent point source energy for the non-ideal blast wave from a fuel-air
and oxygen explosive weapon is three times greater than the energy for a
point blast. Therefore, the far field destructive potential of fuel-air
and oxygen explosive weapons is found to be superior to that of solid ex-
plosive weapons. A detailed discussion and presentaticn of the key results
of this investigation on blast waves from fuel-air explosives are given in
Appendix IV.

In summary our investigations on the transition to detonation,
the influence of confinement on the detonability limits and flame accelera-
tion have provided and are continuing to provide important criteria and
guidelines for both accidental explosions and the development of an FAE III
device. Our understanding of these phenomena are now at the stage where
critical calculations and experiments are being performed. In the case of
FAE III for example, large scale feasibility experiments are being planned
this year.

APPENDIX I

Chemical Initiation of Detonation in Fuel-Air Clouds

1. Pyrophoric Initiation of Detonation in Fuel-Air Mixtures

The present is a summary report of the progress achieved during the fiscal year of 1979 in the investigation of the mechanisms of initiation of detonation in fuel-air mixtures via a chemical catalyst. This work has direct relevance to the development of the single event FAE III device. The main objective of our work at McGill University is a continuing process of research to demonstrate the feasibility of this mode of initiation for the actual realization of an FAE III device based on the co-dispersal of a fuel and a chemical catalyst into air. The approach in the present program is to identify the fundamental underlying mechanisms and to establish quantitative criteria for this mode of initiation on a laboratory scale to be followed up by feasibility demonstration studies in large scale bag tests in collaboration with and at Eglin Air Force Base.

In early 1979 experiments using fluorine injection into heavy hydrocarbon-air mixtures (butane-air, propane-air) were commenced. By mid-1979, direct initiation of detonation in a premixed fuel-air system (propane-air) solely by injecting a chemical catalyst (fluorine) was achieved. A schematic diagram of the apparatus is shown in Fig. 1. In this case charges of fluorine and oxygen (optimum ratio 10% fluorine and 90% oxygen) were counter-injected against a small charge of propane into a premixed reservoir of stoichiometric propane-air mixture. The fluorine interacts with the propane to form an unstable radical (C_3H_7). The oxidation reactions then progress rapidly in the presence of oxygen via a chain-breaking mechanism leading to ignition in the propane-air mixture and ultimately initiation of detonation. No detonation initiation was achieved in other hydrocarbon-air mixtures except propane-air even when these were more detonable than propane-air (eg., ethylene-air). This confirms the effectiveness of the fluorine-heavy hydrocarbon interaction in radical production as indicated

by von Elbe originally. The diagnostics in the present experiments include
a photodiode to detect the onset of chemiluminescent reactions, the signal
from which is used to trigger the oscilloscope. Two pressure transducers
are used to monitor the onset of detonation: one in the vicinity of injec-
tion either above or to the side, the other at the end of the extension tube
as illustrated in the schematic. A typical pressure record illustrating
the case where detonation level pressure was achieved at the end transducer
(upper beam) is displayed in the oscilloscope trace in Fig. 2. The lower
beam illustrates the pressure record in the vicinity of the injection. To
be noted is the fact that it arises later than the pressure spike at the
extension tube end indicating that the development of detonation was in
the region between the injection and the end of the extension tube. This
is compatible with the SWACER mechanism concept of detonation initation.
Thus the feasibility of catalytic detonation initiation in a fuel-air mix-
ture has been demonstrated on the laboratory scale.

2. Criteria for Deconfinement and Scale-up

Laboratory scale experiments of practical necessity must be small
scale and confined. To demonstrate the feasibility of an FAE III single
event device conclusively, large scale unconfined experiments must be ulti-
mately performed. In the present program it is envisioned that these ex-
periments will be carried out at Eglin Air Force Base using bag tests. To
progress from laboratory scale to bag test scale, effects of deconfinement
and scale-up must be considered parametrically. It is well known that deto-
nations in confined tubes can be readily achieved even in the most insen-
sitive fuel-air mixtures (eg., methane-air) as demonstrated by Gerstein and
Kogarko. However, detonation initiation under unconfined conditions is
very difficult in methane-air, requiring large initiating charges of solid
explosive (viz. Bull and Benedick). Thus confinement helps detonation

initiation and propagation. For example, it is well known that if a detonation is initiated and propagates as a well established wave in a confined tube, it may fail when it emerges abruptly into an unconfined geometry unless the diameter of the tube from which the detonation emerged has a diameter greater than some critical tube diameter for the particular mixture. This critical tube diameter for unimpeded transmission of a detonation from confined linear propagation to a fully unconfined geometry has been found to be of great fundamental significance. It can be related to the critical energy for direct initiation of detonation (viz. Lee and Matsui) and is a measure of the geometrical detonability limit which indicates the minimum cross-sectional dimension or thickness of a fuel-air cloud below which a detonation can no longer sustain its steady propagation. A table of experimentally established measurements and estimates of the critical tube diameter for a range of fuel-oxidizer mixtures ranging from fuel-oxygen to fuel-air are presented in Fig. 3. These results indicate that the critical tube diameter for propane-air would be in excess of two meters. This would infer that no detonation propagation would be possible in a propane-air cloud under fully unconfined conditions if the cloud thickness were less than this. However, in the case of a bag test this critical dimension would be somewhat less because of the partial confinement due to ground effect. In the case of a large scale FAE feasibility experiment the implication is that one would have to generate a region of pyrophorically initiated chemical activity which would result in an initiating detonation wave extending over a dimension at least of the order of the critical tube diameter for that particular mixture. Moreover, the energetics of the initiation process would further require that the energy contained in the initiating volume should be at least of the order of the critical energy for direct initiation of detonation in the mixture. These considerations, therefore, provide quantitative guidelines whereby the critical volume of fuel-air mixture which must be pyrophorically

activated for detonation, initiation can be estimated. It is clear that the
initiating volume for propane-air appears to be prohibitively large (i.e.,
a cross-sectional dimension in excess of 2 meters). This would imply that
the catalyst (fluorine-oxygen) would have to be dispersed simultaneously
over a cross-section in excess of 2 meters and perhaps a half meter deep
in the propane-air cloud. Practical problems of the injection process would
therefore appear to preclude propane-air as the FAE cloud. More reasonable
dimensions would indicate that ethylene-air can sustain detonation in a
dimension of cloud less than one meter (i.e., based on a critical tube dia-
meter of 80 cm). Although no critical tube diameter data exist for MAPP-
air or propylene oxide-air mixtures, critical tube diameter values for these
mixtures can be estimated via a simple analysis (viz. Lee and Matsui) from
the critical initiation energy values, say those obtained by Parsons et al.
Based on such estimates MAPP-air would have a critical tube diameter approxi-
mately that of ethylene-air (i.e., 80 cm) while propylene oxide-air would
be even less than that. In terms of an FAE bag test we are therefore talk-
ing of a bag of cross-section slightly in excess of a meter and several
meters long with a pyrophoric injection cross-section of the order of 50-80 cm.
It is important to recall that since the active ingredients for catalytic
initiation are propane, fluorine and oxygen, these constituents must be
provided in the initiating region of the fuel-air vapor cloud which may
now be either ethylene-air, MAPP-air or propylene oxide-air. It is obvious
that for the initiation process to be successful the dispersion time must
be shorter than the catalytic chemical activation time which is typically
short, being of the order of a few milliseconds in this case. Consequently,
in the latter part of 1979, the main efforts in the FAE program at McGill
have concentrated on the study of rapid simultaneous injection and dispersal
techniques via multipoint sources spread over a large cross-sectional area
in anticipation of the approach to be used in the bag test at Eglin Air Force
Base.

3. Rapid Injection, Dispersion and Mixing of Gases

In the original small scale catalytic initiation experiments at McGill, manually activated toggle valves were used successfully for the injection of the pyrophoric constituents into the fuel-air mixture. This proved adequate because only very small regions of chemical activation were involved and the dispersion was sufficiently rapid. In the unconfined large scale bag test context, multipoint simultaneous injection and dispersal on a millisecond time scale would be necessary for reasons already outlined. Clearly the use of remotely activated mechanical toggle valves with their relatively slow opening times and synchronization problems would preclude their use in this case. The requirement for detonation initiation in a bag test would be for very rapid injection, deep penetration, broad lateral spread and intense turbulent mixing of the catalytic ingredients with the fuel-air cloud simultaneously from several injection ports to cover the critical cross-sectional dimension equivalent to the critical tube diameter all on a millisecond time scale. Such requirements would indicate an active rupture type dispersion system and experiments were initiated to study injection of gas charges into an ambient medium via a piston driver-diaphragm scheme (Fig. 4). Argon gas which has virtually the same atomic weight as the fluorine molecular weight was used initially as the injected gas into ambient air for the penetration and dispersion studies. A typical spark schlieren sequence of photographs illustrates a typical injection sequence in Fig. 5. Sufficiently rapid injection and adequate penetration was achieved in this way. Fig. 6 displays typical transient shock-jet trajectories to confirm this. However, when fluorine was subsequently used, its corrosive properties affected the piston sliding trajectory from shot to shot in view of the tight clearances in the honed cylinders required for sealing purposes. Consequently this scheme of injection was deemed too intricate and unreliable for field test

situations. An alternate scheme of simultaneous impulsive rupturing of
an array of prepressurized glass tubes was considered more promising.
I.I. Glass of UTIAS has done considerable work on the gasdynamic flow
field generated from the rupture of cylindrical and spherical pressurized
glass vessels in the early sixties. Of particular interest here is the
very turbulent spread of the contact surface between the pressurized and
ambient gases as a result of the obstructing effect of the shattered
fragments of the glass containers which are initially immobilized because
of their large inertia. The sequence of schlieren photographs in Fig. 7
taken from Glass's book illustrates this. Calculations at McGill using
a gasdynamic numerical code have been carried out for spherical charges
and compared with experimental streak photographs of Glass for identical
initial conditions. The agreement between theory and experiment as indi-
cated in Fig. 8 for the motion of the contact surface is remarkable. The
particular example calculated here is for a practically realistic situa-
tion in the context of an actual bag test. We are contemplating glass
flask charges of pyrophoric gases with gas overpressure ratios of 22-25
(i.e., 325-350 psig). As indicated in Fig. 8, the maximum contact surface
displacement for such overpressure would extend in excess of three times
the initial dimension. For an initial spherical flask dimension of 20-25
cm diameter, the gas would disperse in a time of the order of 500 usec
over a spherical volume in excess of 75 cm diameter. An added advantage
of this mode of dispersion apart from its speed is the fact that the iner-
tia of the shattered glass fragments would provide a "screen" effect
through which the contact front would penetrate and thus become highly
turbulent. This would greatly enhance the rapid mixing capability of the
pyrophoric materials. In an actual bag test initiation experiment it is
contemplated to use three flasks spaced about two flask diameters apart.
The central flask would be pressurized with propane; the other two glass

sphere flasks would contain a pressurized fluorine-oxygen mixture in the ratio of 1:9 fluorine to oxygen. Fig. 9 indicates the sequence of events in the initiation scheme. The central flask containing propane would be ruptured first via mechanical fracture using mild detonating fuse (MDF). The two peripheral flasks containing the fluorine-oxygen charges would then be ruptured in the same way but about 500 µsec later to permit the propane from the first flask to have dispersed to its maximum extent. The subsequent rapid turbulent mixing of the pyrophoric materials over a cross-sectional dimension equivalent to the critical tube diameter for ethylene-air, MAPP-air or propylene-oxide-air mixture in the bag would lead to detonation initiation.
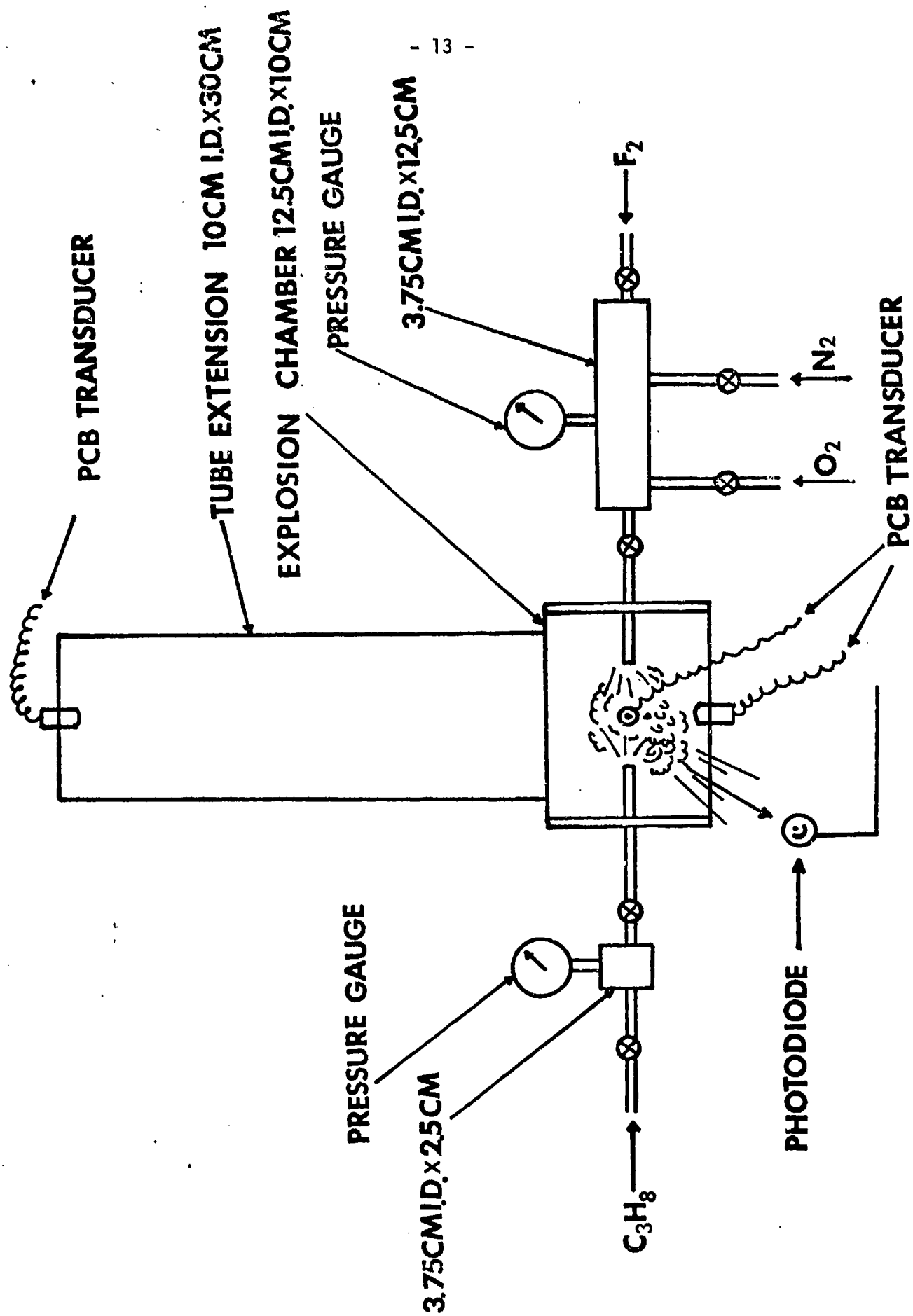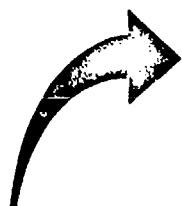
FIG. 1
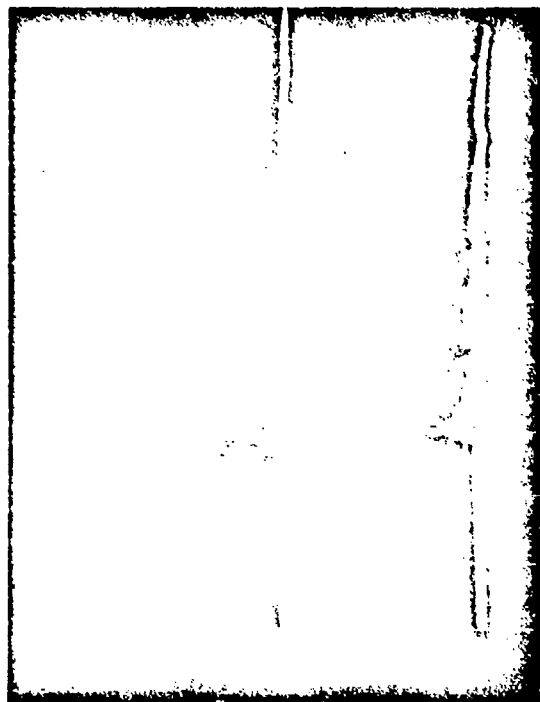
FIG · 2
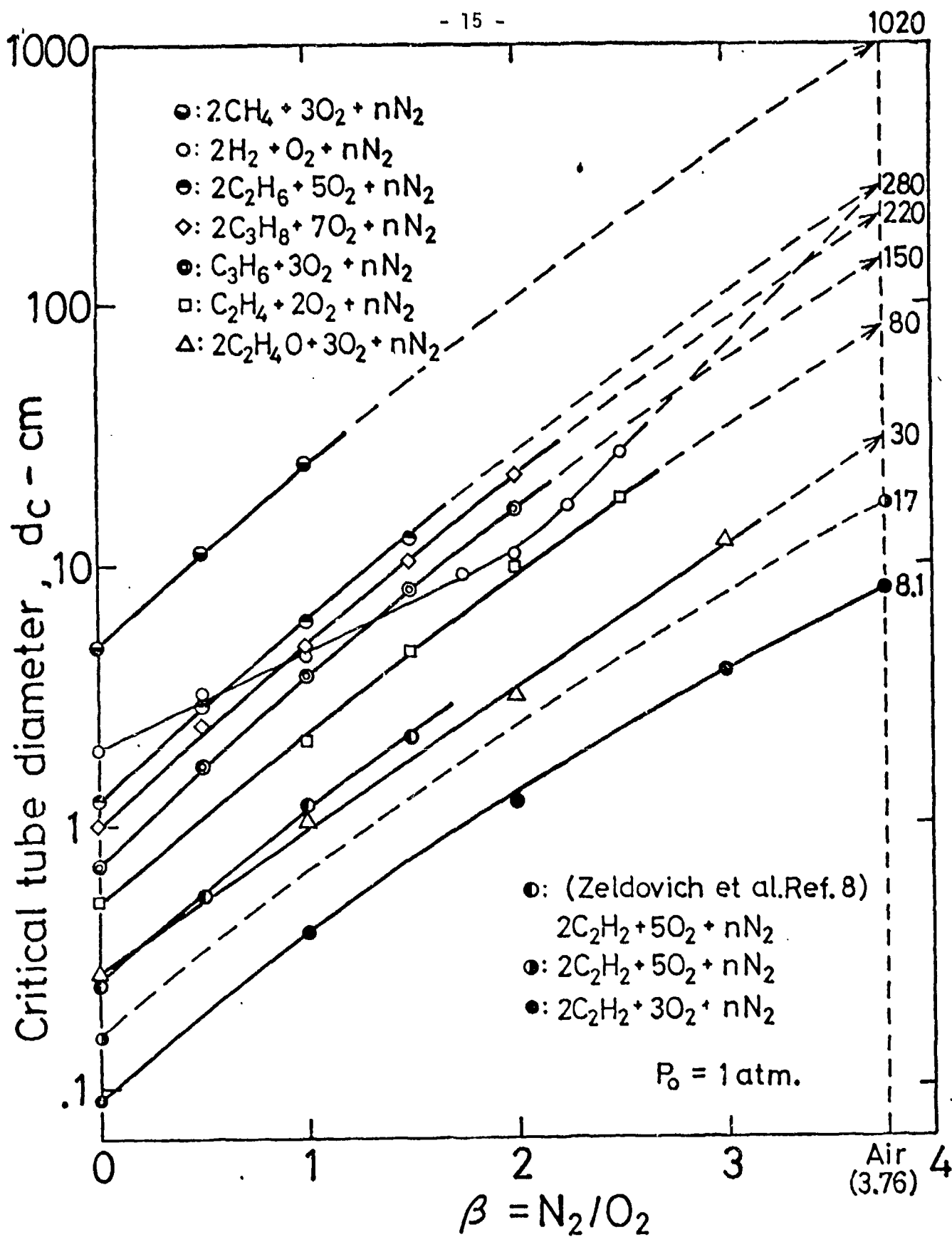
FIG·3
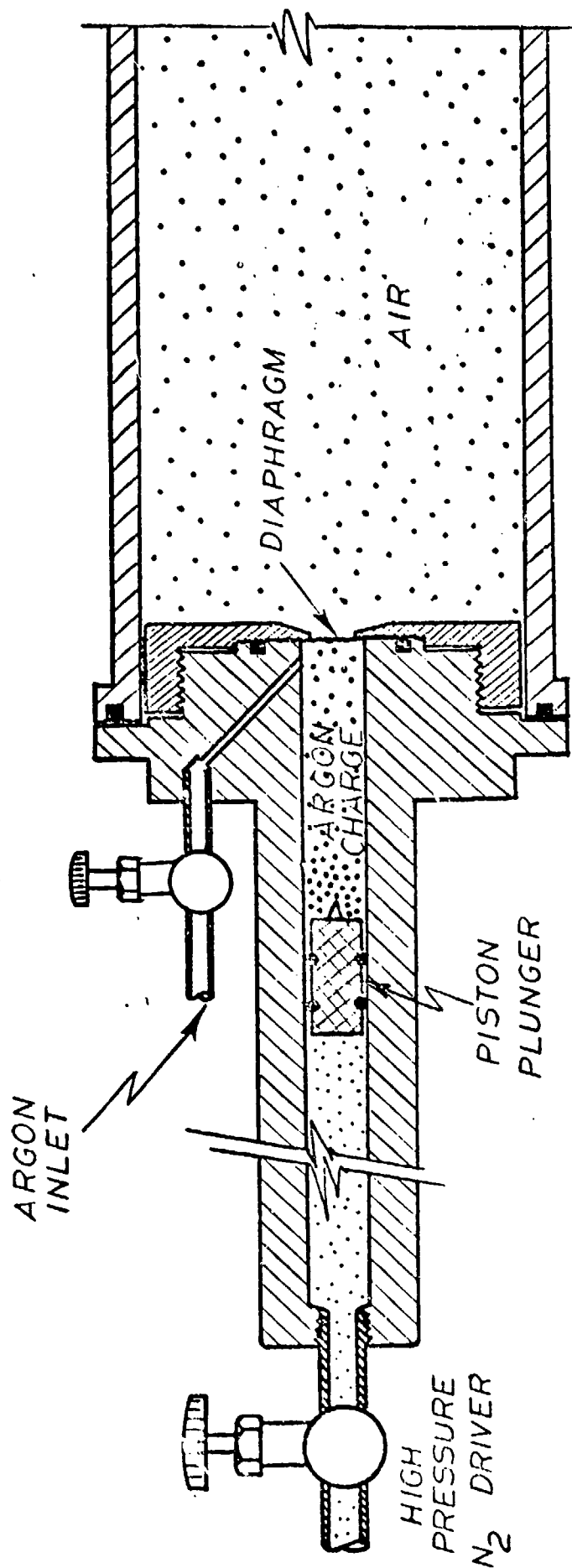
FIG. 4   GAS JET INJECTION APPARATUS

320 μsec
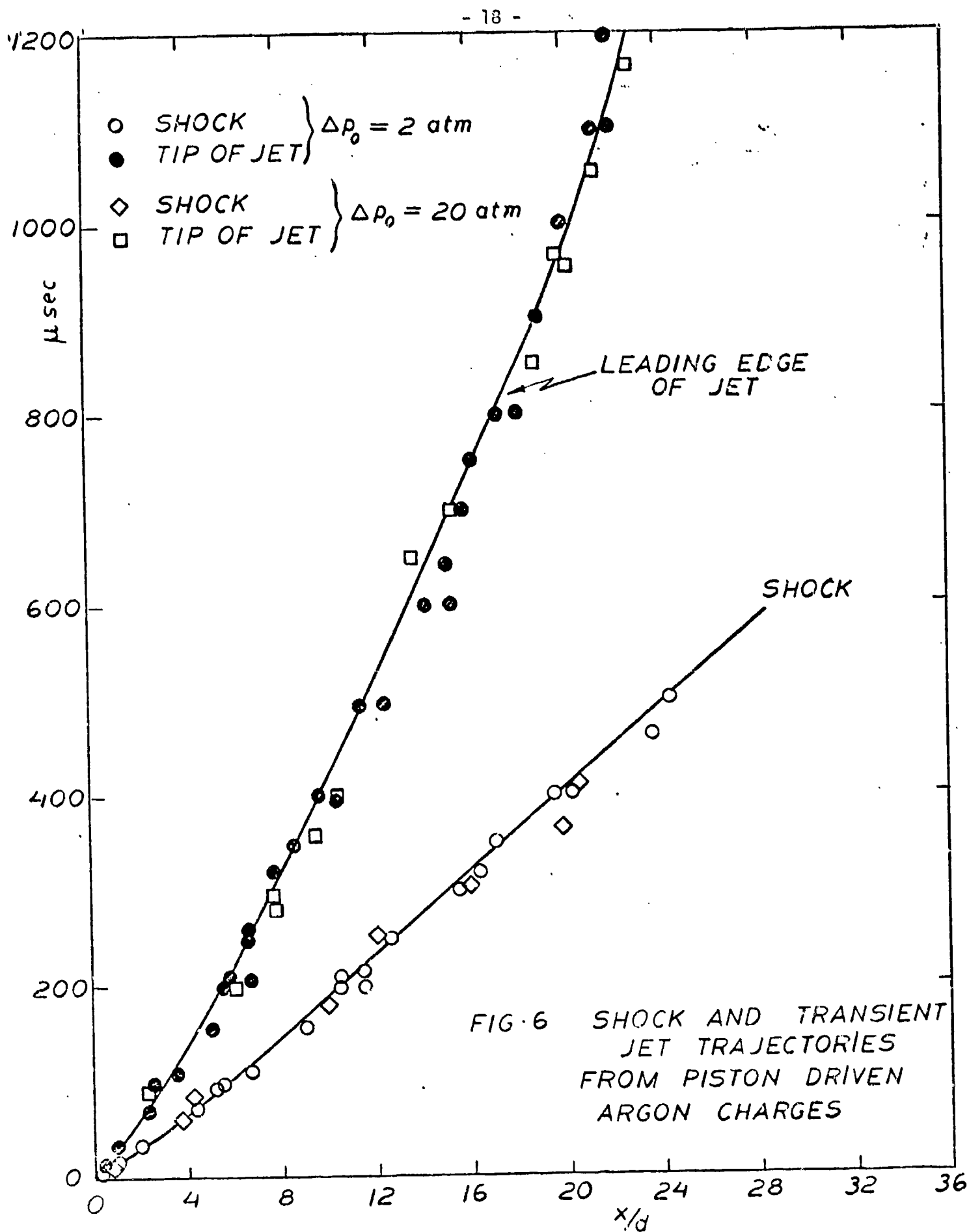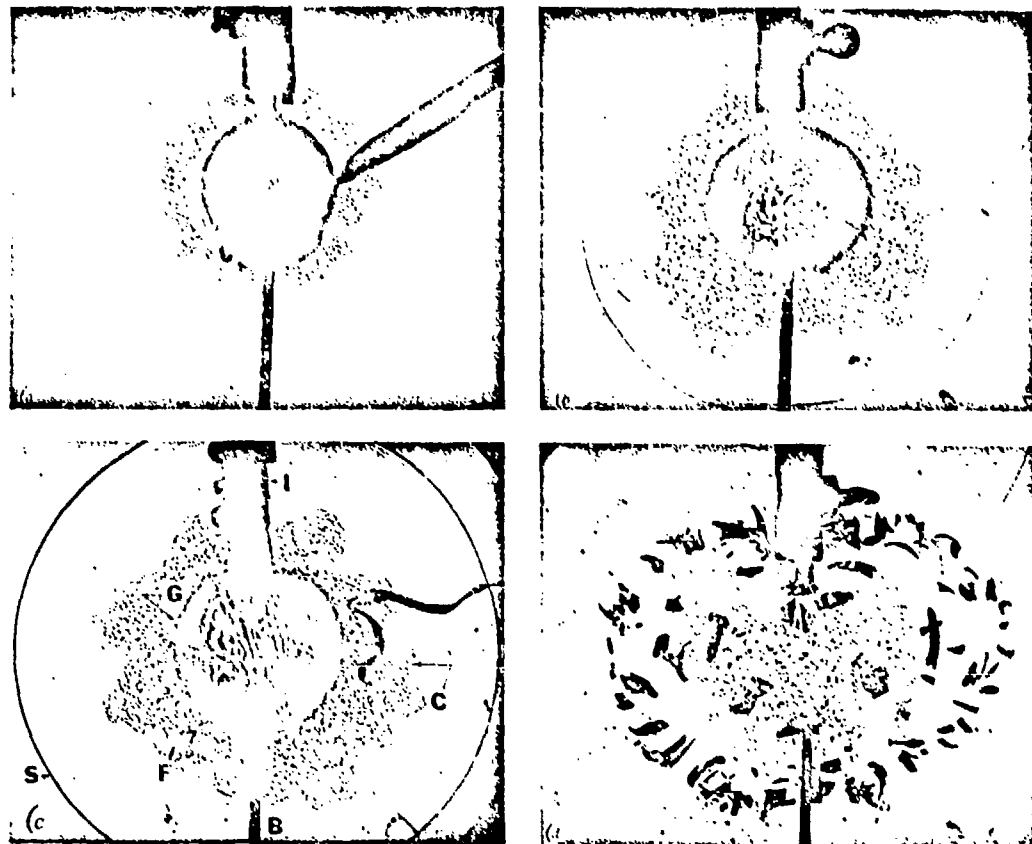
900 μsec

220 μsec

700 μsec

80 μsec

400 μsec

FIG.5
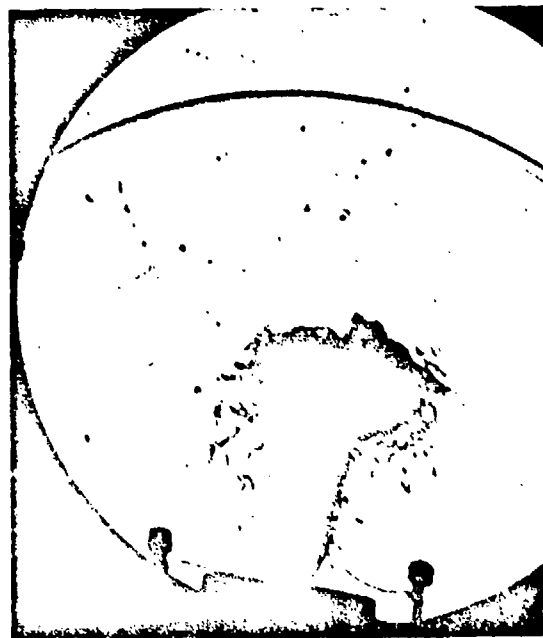
FIG·6 SHOCK AND TRANSIENT
JET TRAJECTORIES
FROM PISTON DRIVEN
ARGON CHARGES

FIG·6

BLAST FROM A PRESSURIZED GLASS SPHERE

FIG·7

BURST OF PRESSURIZED SPHERICAL VESSEL IN AIR

$$\frac{P_4}{P_1} = 22 \qquad \frac{T_1}{T_1} = 1$$

R_0 : RADIUS OF VESSEL

FIG·8
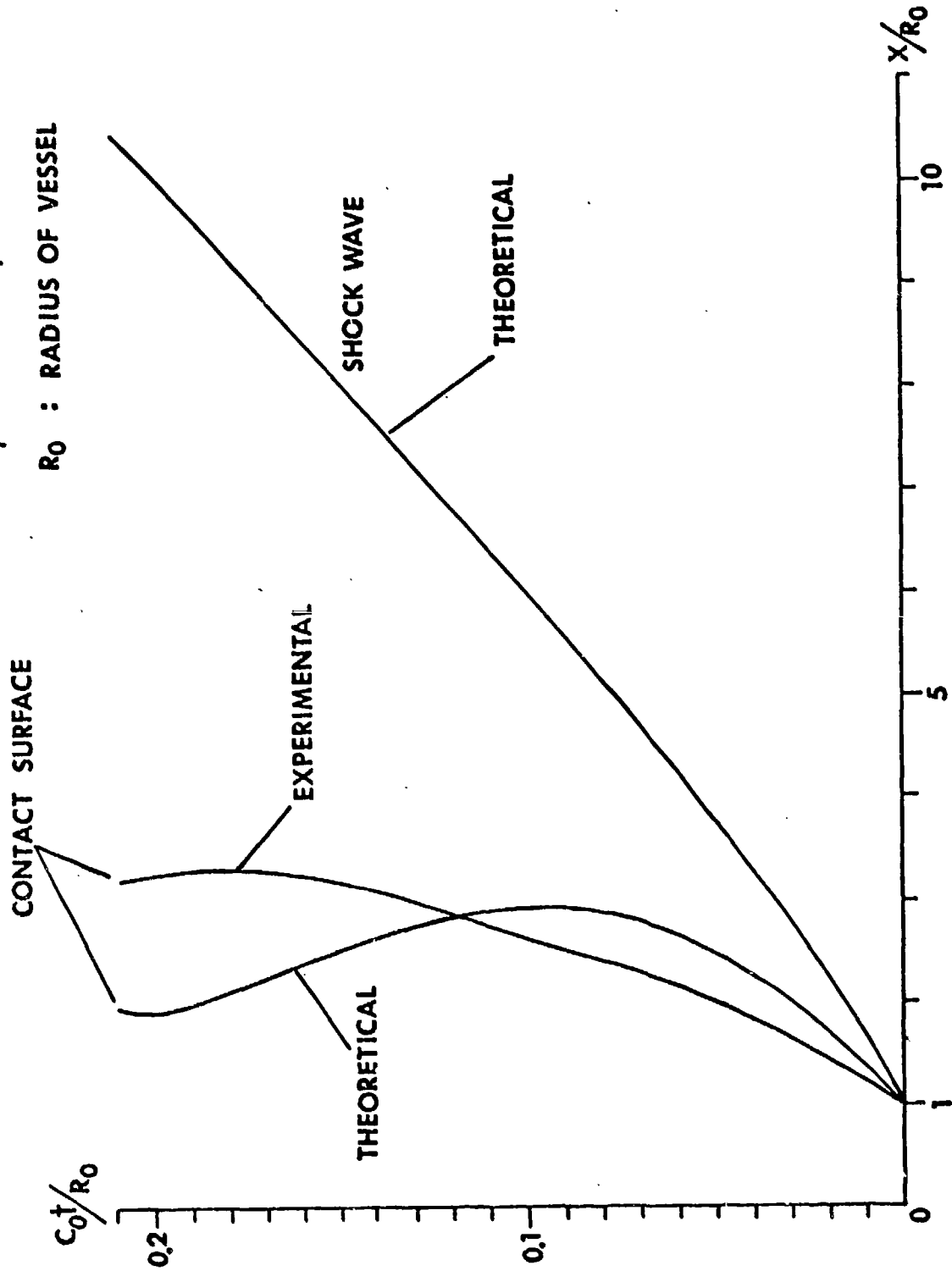
PRESSURIZED GLASS FLASKS

$F_2 + O_2$

MDF IMPACT SHATTERING

C_3H_8

$F_2 + O_2$

FUEL-AIR BAG

(1)

SHOCK

TURBULENT CONTACT FRONT
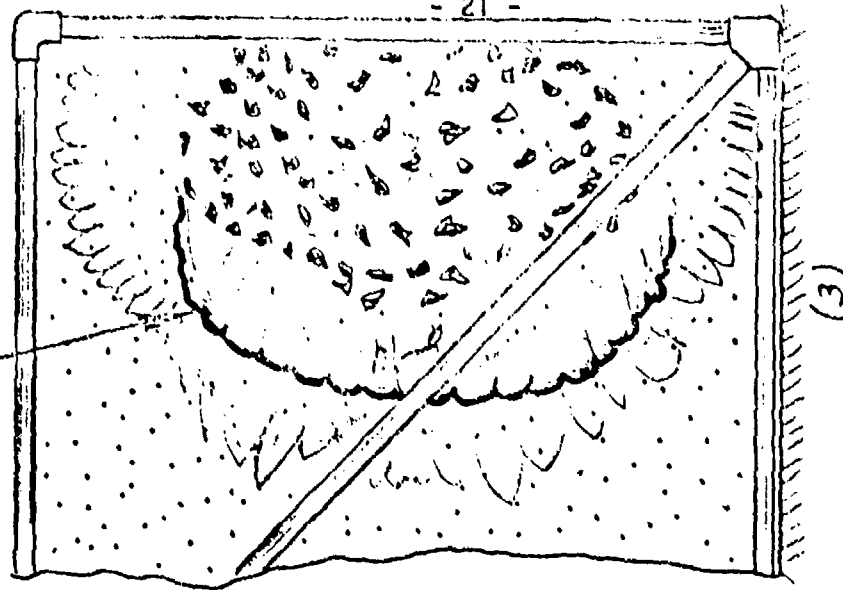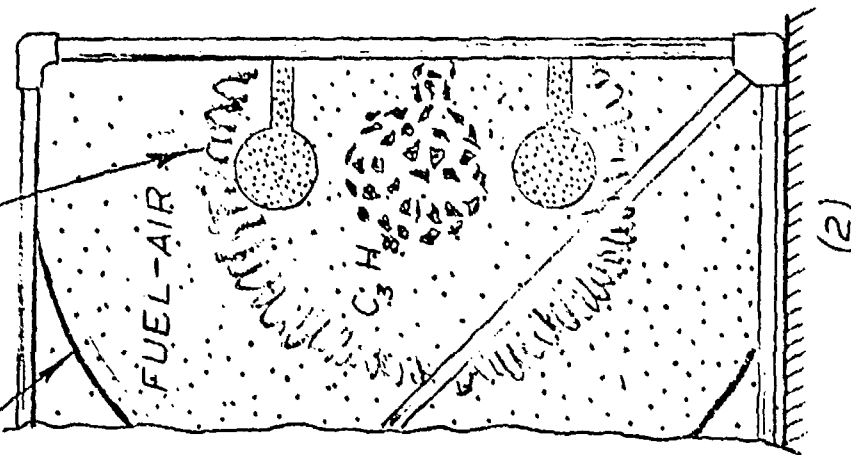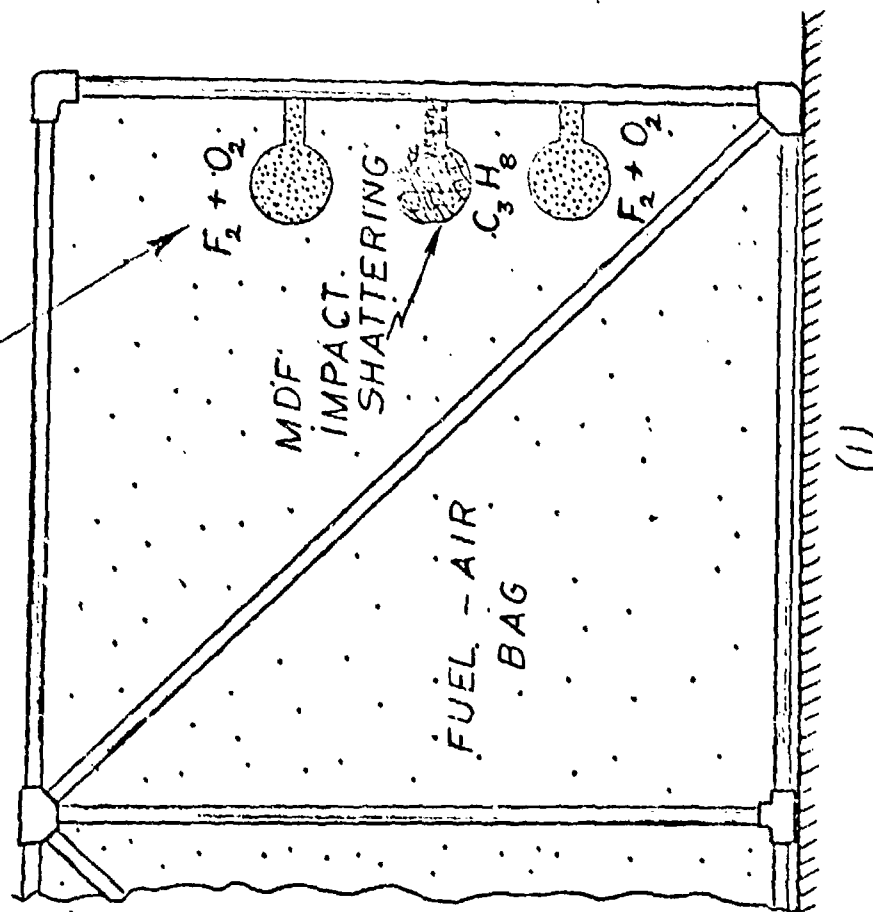
FUEL-AIR

C_3H_8

(2)

DETONATION

(3)

FIG.9 PYROPHORIC DETONATION INITIATION IN FUEL-AIR BAG TEST

FIG.9

APPENDIX II

Turbulent Flame Propagation and Acceleration
in the Presence of Obstacles*

* Paper submitted to the Proceedings of the VIIth International Colloquium
on Gasdynamics of Explosions and Reactive Systems.

1. Introduction

Violent flame acceleration and enhanced transition to detonation when turbulence producing obstacles are placed in the path of a flame have been observed by various authors.[1-3] However, at the present time, the questions of maximum flame speed and flame acceleration in unconfined or partially confined situations with turbulence producing obstacles and/or initial turbulence are still far from being resolved. From the practical point of view it is important to determine the flame acceleration and maximum flame speed for a wide range of turbulence conditions since the turbulence in a cloud of combustible mixture, which may result from an accidental spill of explosive gases and liquids, can vary widely depending on the nature and location of the spill. Even if the turbulence level is low prior to ignition, the presence of obstacles in the form of buildings, vehicles, pipes, etc., can lead to large flame speeds and potentially dangerous blast waves.

At the present time, flame laws relating the flame speed of a freely propagating flame to the turbulence field or obstacle configuration are not available. Such flame laws are required as input to existing numerical gas-dynamic calculations[4-6] to evaluate the resulting pressure waves, so that the blast effects due to a fuel-air explosion in a turbulent environment can be predicted. We have undertaken a program whose aim is to develop such flame laws.

In a previous paper[7] we reported on the dramatic acceleration of cylindrically expanding methane-air flames when repeated obstacles were placed in the flame path. With repeated obstacles of the appropriate sizes and separations, flame speeds up to 130 m/s were obtained. This was approximately 24 times the speed observed with no obstacles. The mechanism proposed for the rapid acceleration of the flame from an initial flame speed of about 3.3 m/s to speeds in excess of 100 m/s over a distance of 30.5 cm was based on the

positive feedback coupling between the flame and the upstream flow produced
by the specific volume increase across the flame. With repeated obstacles
in the flame path, gradients in the upstream flow field produce "flame fold-
ing" which increases flame area and hence the rate of burning, leading to a
larger flow velocity and stronger flow field gradients, which then further
increases the rate of burning and so on. This positive feedback mechanism
can thus lead to a flame which, without some damping or limiting factors,
will continue to accelerate as long as the obstacle configuration remains
the same.

Most of the results reported in Reference 7 were based on experi-
ments in a chamber which provided only 30.5 cm of flame travel. A few ex-
periments were performed in a larger chamber providing 61 cm of flame travel.
These latter experiments confirmed the dramatic influence of obstacles on
the flame propagation, but the results were inconclusive on the questions of
continued flame acceleration and maximum flame speed. To investigate these
questions further we constructed a larger chamber so that cylindrical flame
propagation could be observed over a distance of 120 cm. This paper reports
on the results of this investigation. Based on these results together with
spark schlieren photographs of the flame propagation over obstacles in a rec-
tangular channel, a simple model of the flame acceleration process is pro-
posed. This model predicts an exponential increase in flame speed with dis-
tance propagated over obstacles which is in good agreement with the experi-
mental results.

2. Experimental Details

The investigation of flame propagation over obstacles was performed
in a 2.5m x 2.5m chamber consisting of two wooden parallel plates separated
by spacers at the corners. The plate separation could be adjusted by changing

the spacers. The chamber was sealed at the periphery by plastic bands while it was filled with the appropriate gas mixture. A spring mechanism was used to remove these plastic bands prior to ignition so that the flame could expand freely in the radial direction. The gas mixture of stoichiometric methane-air was prepared by continuous flow, and the chamber was purged at least 10 times in order to ensure a good mixture in the chamber. Ignition was achieved by a fast burning wire at the center of the chamber, and the subsequent radial propagation of the flame was recorded by a rotating drum streak camera. A schematic diagram of the experimental set-up is shown in Figure 1.

The obstacle configurations were identical to those used in the laboratory experiments reported in Reference 7, with obstacles consisting of spirals of copper or plastic tubing. The spiral obstacles were placed on the top or bottom plate so that a radially expanding flame would encounter a series of obstacles, corresponding to the windings of the spirals, which extended all the way to the periphery of the chamber. A cross-sectional slice through the center of the chamber illustrating the obstacle configurations is shown in Figure 2. The obstacle height H, the pitch P and the plate separation D are also defined in this figure. For these particular experiments two types of obstacle spirals were used; i) a spiral of 1.25 cm diameter copper tubing with a pitch of 3.75 cm, and ii) a spiral of 4 cm plastic tubing with a pitch of 10 cm. The plate separation was varied between 3.5 cm and 20 cm.

To investigate in more detail the mechanism of flame propagation over obstacles we have also taken schlieren photographs of a methane-air flame propagating over obstacles in a rectangular channel of length 30 cm. This channel was constructed by placing wooden bars in the 30.5 cm radius chamber described in Reference 7, and the schlieren photographs were taken through windows in the two plates of the chamber. A schematic diagram of

the channel with obstacles is shown in Figure 3, where the relevant parameters; pitch (P), obstacle diameter (H) and channel width (W) are also defined. The height of the channel was 2.54 cm. For some of the experiments in the channel one or more of the obstacles were filled with dry ice. Three small holes in these obstacles allowed CO_2 to escape. The escaping CO_2 provides an excellent schlieren tracer for the flow field ahead of the flame.

3. General Considerations

As discussed in Reference 7, the dramatic influence of repeated obstacles on the flame propagation can be understood in terms of the positive feedback coupling between the flame itself and the flow ahead of the flame. When obstacles are placed in the flame path, the upstream flow field will be that characteristic of the obstacle configuration. For repeated obstacles placed on the bottom and/or top plates of the chamber, the main features of the flow ahead of the flame are a standing eddy in the wake region behind the obstacles which is separated from the outer flow region by a shear layer. The flow pattern ahead of the flame and the entrainment into the standing eddy for low flame velocities is illustrated by the spark-schlieren photograph shown in Figure 4a. In this case the second and the fourth obstacles have been filled with dry ice and the resulting CO_2 tracer clearly shows a standing eddy region between the second and third obstacle. As the flame encounters this flow field it will become "folded" due to the gradient in the flow field, leading to a flame consisting of a curved leading flame front in the outer flow region with a trailing flame in the standing eddy between the obstacles. This is illustrated in the spark schlieren photograph shown in Figure 4b. This photograph also shows the entrainment of the flame zone into the eddy. For larger flame speeds and thus larger flow velocities ahead of the flame, the shear layers and the wakes of the obstacles will become turbulent and as the

velocity increases the turbulent flow region will encompass more and more of the flow field. This is illustrated in Figure 5a where dry ice in the fourth obstacle provides the CO_2 tracer. The turbulent wrinkling and entrainment of the flame zone into the wake region can also be seen in this figure. The smaller scale turbulent wrinkling of the flame is further illustrated by the spark-schlieren photograph shown in Figure 5b. These spark-schlieren photographs confirm the picture of flame propagation over obstacles proposed in Reference 7. A schematic diagram illustrating this physical picture is shown in Figure 6.

As discussed in Referene 7, the turbulent burning velocity S_T based on the average heat release rate per unit projected or frontal flame area is given by:

$$S_T = \frac{1}{2\pi rD} \int S da,$$

$$(1)$$

where the integral is over the area of the "flame fold" shown in Figure 6, S is the local burning velocity at the "flame fold" surface, D is the plate separation and r is the radial position of the flame front. Assuming zero flow velocity in the unburned gases behind the flame, the displacement velocity of the unburned gases just ahead of the flame averaged over the plate separation is given by:

$$\langle V_u \rangle = \left(\frac{\rho_u}{\rho_b} - 1 \right) S_T$$

$$(2)$$

where ρ_u and ρ_b are the average densities of the unburned gas ahead of the flame and the burned gas behind the flame zone, respectively. Thus, assuming that the advance of the flame is uniform across the plate separation and that transient effects can be neglected, the corresponding flame speed is given by

$$\dot{R}_f = \frac{\rho_u}{\rho_b} S_T.$$

$$(3)$$

For low flame speeds in the initial stages of the flame acceleration, the flame acceleration mechanism is clearly "flame folding" due to the gradient in the mean flow field produced by the obstacles. The turbulent burning velocity S_T is enhanced by an increase in relative flame surface area (i.e., relative to the projected flame area $2\pi r D$) as the flame is stretched in the mean flow gradient field. As the burning velocity increases the flow velocity ahead also increases leading to more intense "flame folding", thus to a larger burning velocity and so on. Superimposed on the large scale "flame fold" is the smaller scale turbulent flow field which leads to flame wrinkling and increased rate of turbulent transport of heat and mass across the "flame fold" surface. The resulting increase in burning velocity at the "flame fold" surface or increase in "flame fold" burning rate leads to a further increase in turbulent burning velocity. During these initial stages the flame acceleration will be determined mainly by the rate of "flame folding". However, as the flame accelerates, the smaller scale turbulent flow field in the wakes and shear layer regions will begin to play a more important role in the acceleration process. As observed in Figure 5, the burning in the wake regions will become less well defined due to smaller scale and larger intensity turbulent entrainment and mixing, and the main flame front will become wrinkled as the turbulence in the wake regions spreads into the main flow region.

Transition to turbulence in the wake of a cylinder occurs at Reynolds numbers above 200 and the location of the transition point moves towards the cylinder as the Reynolds number increases.[8,9] Even for very low flow velocities ~10 m/sec with 1.25 cm obstacles the Reynolds number is more than 8000 so that the wake of the obstacles will always be turbulent. The acceleration of the flame thus depends on both the rate of growth of the "flame fold" relative to the projected area $2\pi r D$ and on the increase in the "flame fold" burning rate. In the initial stages of the flame acceleration, where the mean flow velocity is low, the dominant mechanism is the rate of growth of the "flame

"fold". But as the flame speed increases, the folded area for a given obstacle configuration will approach some asymptotic maximum since the flame cannot be stretched out indefinitely. Beyond this, the flame acceleration will depend more on the small scale turbulence intensity which governs the burning rate of the "flame folds". The small scale turbulence derives its energy from the shear flow gradient of the mean flow field, thus the flame speed will be governed by the rate in which the fine scale turbulence can derive its energy from the mean shear flow. For the initial stages of the flame acceleration where the development of the "flame fold" dominates, a computer simulation of the transient inviscid flow structure should be adequate for determining the flame acceleration due to "flame fold" area increase. For the later stages of the flame acceleration, when the folded structure approaches some steady value and small scale turbulence dominates subsequent flame acceleration, it should be possible to model the acceleration analytically by postulating a dependence of the burning velocity on small scale turbulence. In this paper we shall propose a simple feedback mechanism for the latter stages of the flame acceleration based on the assumption that the increase in the rate of burning of the "flame fold" controls the acceleration process. The details of the initial flame acceleration leading to the establishment of the "flame fold" will not be considered.

4. Results and Discussion

According to Townsend[10] the turbulence intensity u'/u_0 in a plane wake is of the order of 0.4, where u' is the root mean square turbulent velocity and u_0 is the mean velocity variation across the wake. If we take u_0 as one half the maximum flow velocity ahead of the flame, we obtain a turbulent velocity $u' \sim 0.2 \dot{R}_f$ in the wake of the obstacle ahead of the flame. Townsend's conclusions are based on fully developed turbulent flow in the far wake region

of an obstacle in an infinite stream, but the estimate of $u' \approx 0.2 \, U_{max}$ ($\approx 0.2 \, \dot{R}_f$) in the near wake regions of bluff obstacles in a boundary layer is supported by measurements by Chang,[11] Counihan, Hunt and Jackson,[12] and by recent measurements in our laboratory. Townsend also quotes a value of $u_e \approx 0.21/u_0$ (i.e., $\approx 0.1 \, R_f$) for the entrainment velocity, i.e., rate at which non-turbulent fluid flows through the bounding surface of the wake and becomes turbulent. Thus as the speed of the flame increases, both the r.m.s. turbulent velocity and the rate at which the unburned gas ahead of the flame is made turbulent increases.

To model the feedback mechanism based on increase in "flame fold" burning rate due to this increase in turbulence with flame speed, let us focus on the region around the nth obstacle and denote the average speeds of the flame front through the regions just before and just after this obstacle by $\dot{R}_f(n-1)$ and $\dot{R}_f(n)$, respectively. These flame speeds will be determined by the respective turbulent burning velocities, which according to our previous discussion depend on both the relative size of the "flame fold" and on the "flame fold" burning rate. If the relative size of the "flame fold" (i.e., relative to the projected area $2\pi r0$) remains the same, the increase in flame speed is due solely to an increase in "flame fold" burning rate, i.e., increase in effective burning velocity at the "flame fold" surface. Making the assumption that this burning rate is proportional to $(u')^\beta$ (for the correlation proposed by Abdel-Gayed and Bradley[13] for high intensity isotropic turbulence, for example, $\beta = 0.238$) we find that

$$\dot{R}_f(n) = \dot{R}_f(n-1)\left[1 + \beta \, \frac{\Delta u'}{u'}\right] \tag{4}$$

where $\Delta u'/u'$ is the relative increase in turbulence due to the presence of the obstacle, and we have assumed that $\Delta u'/u' \ll 1$.

The increase in turbulence in the developing wake region will not

be uniform throughout the region between the obstacles, but will develop from an initial transition point which depends on the Reynolds number of the flow and the initial turbulence[8,9] and spread as more of the outer stream fluid is engulfed into the wake. For the flame speeds we are concerned with, the initial turbulence and Reynolds numbers are sufficiently large so that transition can be considered to occur right at the obstacle itself. Hence, $\delta u'/u'$ which represents the relative increase in turbulence averaged over the entire region between the obstacles will depend on the separation of the obstacles and on the blockage ratio H/D. If we assume a linear growth of the region with increased turbulence in the near wake and a power dependence on H/D we obtain a relation of the form

$$\dot{R}_f(n) = \dot{R}_f(n-1)\left[1 + \frac{\text{p}}{\text{L}}\left(\frac{H}{D}\right)^a\right],\tag{5}$$

between the average flame speeds before and after the nth obstacle, where a is a constant and L is a length which characterizes the growth of the turbulent region. The assumption of linear growth of the turbulent region in the near wake region is rather arbitrary, but as we shall see this assumption does give the correct scaling from obstacle configurations with $p = 3.75$ cm to obstacle configurations with $p = 10$ cm. Although Equation (5) has been obtained by focussing on the regions just before and just after the nth obstacle, the result does not depend on the relative size of the "flame fold". As long as the relative size of the "flame fold" remains the same and the relative increase in turbulence depends on the obstacle configuration only, exactly the same arguments apply for any size "flame fold".

Since the above mechanism does not include the contribution to flame acceleration due to increase in the relative size of the "flame fold" it cannot describe the initial acceleration. However, if we assume that the increase "flame fold" burning rate dominates the flame acceleration process after the

flame has propagated over n_0 obstacles, then for $n > n_0$ we can use Equation 5 to obtain the following relation

$$\dot{R}_f(n) = \dot{R}_f(n_0)[1 + \frac{p}{p_0}(\frac{H}{D})^\alpha]^{(n-n_0)},\qquad(6)$$

for the flame velocity after the nth obstacle, where we have defined $p_0 = L/\beta$. For small p the above relation becomes

$$\dot{R}_f(r) = \dot{R}_f(r_0)\exp[\frac{(r-r_0)}{p_0}(\frac{H}{D})^\alpha].\qquad(7)$$

In other words, it is predicted that the flame velocity increases exponentially with r for $r > r_0$. As can be seen in Figure 7, this prediction is supported by the experimental results. If r_0 is chosen at 60 cm with $\alpha = 0.31$ and $p_0 = 37.5$ cm, Equation 7 provides a good correlation of the experimental results from all the experiments with obstacle configurations which include the 1.25 cm copper tube spiral. In fact, for those experiments with copper tube spiral obstacles only, the correlation is good down to about 30 cm of flame travel. The prediction for the larger 4 cm obstacles with the same parameters α and p_0, using Equation 6 rather than Equation 7 since the exponential approximation is not valid in this case, is shown in Figure 8. Again, agreement with the experimental results is quite good for $r \gtrsim 60$ cm (i.e., n ~ 5), but significant deviations are clearly observed for $r < 60$ cm.

The transition from flame acceleration dominated by the rate of flame fold growth to acceleration dominated by the increase in "flame fold" burning rate is clearly not a sharp one. There will be a transition region where both mechanisms are equally important, and in this region the flame acceleration is expected to be greatest. That the initial acceleration of the flame is greater than that predicted by Equations 6 and 7 is clearly evident in both Figures 7 and 8. Note that for r = 0 all the curves should converge to an initial flame velocity of 3.3 m/s. Once the increase in "flame

"fold" burning rate begins to dominate the acceleration process a simple model of the feedback mechanism based on a positive feedback coupling between the turbulence produced by the obstacles and the flame speed predicts an exponential increase in flame speed which agrees well with the experimental results. In fact, Equation 4 which relates the change in flame speed to the change in turbulence can be applied more generally. It would predict, for example, that the flame will slow down if there were no obstacles beyond a certain distance; the change in turbulence intensity $\delta u'$ would then eventually become negative and the flame would decelerate. Furthermore, the parameters p_0 and α, in particular p_0, would be expected to depend on geometry (i.e., planar, cylindrical or spherical) and to be constant only in a certain range of p/H.

The predicted exponential increase in flame speed cannot continue indefinitely. As the flame speed increases the strength of the shock waves produced will increase and shock wave heating combined with turbulent mixing may lead to auto-ignition near the leading shock wave, in which case a coupled shock wave reaction zone complex may continue to propagate at a constant velocity characteristic of the obstacle configuration. Such coupled complexes with velocities depending on the obstacle configuration but much smaller than the C-J detonation velocity have been observed by man, authors.[1,13-15] Another possibility is that the rate of chemical reaction becomes the limiting factor. As the flame speed increases the intensity of the turbulence in the regions between obstacles increases, leading to the observed exponential flame acceleration. However, there is a maximum mass rate at which a given volume of a combustible gas at a given pressure can burn, this corresponds to the well stirred reactor. Thus at a certain turbulence intensity chemistry begins to play a role. If the rate of turbulent mixing exceeds the rate at which the mixture can burn the flame may be temporarily blown out or locally quenched. Such quenching has been observed by Wagner and collaborators,[16] for example.

Our experimental results which include flame speeds larger than 400 m/sec for stoichiometric methane-air mixtures show no indication that the flame speed is approaching a maximum value. Thus we would expect the flame to continue to accelerate to even larger flame speeds if the obstacle configuration was continued.

The maximum flame speed observed with no obstacles in the chamber was 9 m/sec, and no acceleration was observed in the last 20 cm of propagation. This is almost twice the value observed in the 30.5 cm radius chamber in the laboratory.[7] The difference can be attributed to additional surface roughness of the wooden plates and slight variation in plate separation due to sagging of the top plate. The plate separation varied by as much as 1 cm over the area of the chamber. This variation of plate separation also accounts for the fact that the flame speeds at 30 cm were typically larger than those observed in the smaller laboratory chamber for the same obstacle configuration. For H/D = 0.34 with 1.25 cm copper tubing obstacles, for example, the speed at 30 cm is 45 ± 5 ms to be compared with about 30 m/s observed in the laboratory experiments with the same obstacles at this H/D. The variation in D due to sagging leads to an uncertainty in H/D of 0.06, and if this uncertainty is taken into account the two results are in agreement.

The strength of the shock waves produced by these fast turbulent flames were not measured in a systematic manner, but two pressure transducers at the periphery of the chamber were used to record the shock wave overpressures in some of the experiments. For the fastest flame with a maximum flame speed of 415 m/sec a shock wave overpressure of 0.64 bar was obtained. According to the steady-state analysis of Guirao et al.[6] this would correspond to a constant burning velocity of about 35 m/s to be compared with a maximum turbulent burning velocity of 55 m/s obtained using Equation 3 with a density ratio of 7.5. Similarly, for the flame with maximum velocity 305 m/s the

measured shock overpressure was 0.27 bar, which according to Guirao et al. corresponds to a constant burning velocity of about 28 m/s to be compared with a maximum turbulent burning velocity of 41 m/s obtained from Equation 3. In view of the dramatic acceleration of the flames observed in both of these cases the disagreement with steady state calculations based on constant burning velocity is not surprising. Strehlow et al.[5] have recently shown that calculations using constant velocity flames based on the maximum effective burning velocity of accelerating flames can lead to an overestimate of the maximum overpressure. Furthermore, Equation 3 which we have used to calculate the turbulent burning velocity may have to be modified for violently accelerating flames. The agreement with steady state analysis is much better for the slower flames. For the flame with maximum speed of 150 m/s, for example, the measured shock overpressure is 0.062 bar corresponding to a steady state burning velocity of about 17 m/s to be compared with 20 m/s obtained from Equation 3.

5. Conclusion

The influence of repeated obstacles on freely expanding stoichiometric methane-air flames in cylindrical geometry has been investigated in a chamber where the flame propagation could be observed over a distance of 120 cm. This investigation confirms the dramatic influence of obstacles on the speed of the flame reported previously and shows that with repeated obstacles the flame speed continues to increase up to speeds in excess of 450 m/sec. The shock waves generated by these fast turbulent flames have overpressures up to 0.64 bar, which could lead to extensive blast wave damage.

The mechanism responsible for the rapid acceleration of the flame in an obstacle environment can be understood in terms of the positive feed-back coupling between the flame and the upstream flow produced by the specific

volume increase across the flame. The physical picture of this positive feedback mechanism proposed in a previous paper[1] is confirmed by spark-schlieren photographs of the flame propagation over obstacles in a rectangular channel.

The acceleration of the flame depends on both the rate of growth of the "flame fold" relative to projected flame area and on the increase in the "flame fold" burning rate. In the initial stages of the flame acceleration the dominant mechanism is the rate of growth of the "flame fold", but as the flame speed increases the rate of increase in the "flame fold" burning rate begins to dominate the flame acceleration process. A simple feedback mechanism is proposed for the latter stages of the flame acceleration, based on the assumption that the increase in the rate of burning of the "flame fold" due to the turbulence produced by the obstacles controls the acceleration process. This model assumes that a "flame fold" (which does not continue to grow) has already been established, and that the rate of burning of this "flame fold" is determined by the turbulence field which the flame propagates into. The details of the turbulent combustion or the nature of the combustion zone are not considered. The model predicts an exponential increase in flame speed with distance propagated over obstacles, which is in good agreement with the experimental results. Although this exponential increase cannot continue indefinitely, no evidence that the flame speed is approaching a limiting value was found in the present experiments.

The details of the initial acceleration of the flame which involves both "flame folding" and increase in "flame fold" burning rate due to turbulence or the critical size of the "flame fold" for which the rate of growth of the "flame fold" can be neglected cannot be determined from the present analysis. A more detailed model of the flow field produced by the accelerating flame propagation over obstacles and of the flame-turbulence interaction

is required to describe the initial flame acceleration and to estimate the size of the flame fold. Investigations with the aim of developing such a model are now in progress.

References

1. Shchelkin, K.I., Journal of Experimental and Theoretical Physics (USSR) 10, 823 (1940).

2. Chapman, W.R. and Wheeler, R.V., J. Chem. Soc. 1926, 2139 (1926).

3. Dörge, K.S., Pangritz, D. and Wagner H.Gg., Acta Astronautica 3, 1069 (1976).

4. Kurylo, J., Dwyer, H.A. and Oppenheim, A.K., "Numerical Analysis of Flow Fields Generated by Accelerating Flames", paper 79-0290, AIAA 17th Aerospace Meeting, New Orleans, Jan. 15-17, 1979.

5. Strehlow, R.T., Luckritz, R.T., Adamczyk, A.A., and Shimpi, S.A., Combustion and Flame, 35, 297 (1979).

6. Guirao, C.M. Bach, G.G., and Lee, J.H., Combustion and Flame, 27, 341 (1976).

7. Moen, I.O., Donato, M., Knystautas, R., and Lee, J.H., "Flame Acceleration Due to Turbulence Produced by Obstacles", McGill University Preprint 1979.

8. Bradshaw, A., "On the Development of Turbulent Wakes from Vortex Streets", NACA Report 1191 (1954).

9. Papailiou, D.D., and Lykoudis, P.S., Journal of Fluid Mechanics, 62, 11 (1974).

10. Townsend, A.A., "The Structure of Turbulent Shear Flow", 2nd edition, Cambridge University Press, Cambridge 1976.

11. Chung, S.C., "Velocity Distributions in Separated Flow Behind a Wedge-Shaped Model Hill", Colorado State University, Denver, Colorado, 1966 (unpublished); see Plate, E.J., Agricultural Meteorology, 8, 293 (1971).

12. Counihan, J., Hunt, J.C.R., and Jackson, P.S., Journal of Fluid Mechanics, 64, 529 (1974).

13. Abdel-Gayed, R.G. and Bradley, D., Sixteenth Symposium (International) on Combustion, The Combustion Institute, Pittsburgh, Pa. (1977), p. 1725.

14. Guenoche, H., and Manson, N., Revue de L'Institut Français du Petrole, No. 2, 53 (1949).

15. C. Brochet, "Contribution à L'étude des Détonations Instables dans les Mélanges Gazeux", Thèses présentées à la Faculté des Sciences de L'Université de Poitiers, 1966, Chapter VI, pp. 107-121.

16. Dörge, K.S., Pangritz, D., and Wagner, H.Gg., "Influence of Obstacles on the Propagation of Flames", paper presented at the VIIth International Colloquium on Gasdynamics of Explosions and Reactive Systems, Göttingen, West Germany, 20-24 August, 1979.

Figure Captions

Figure 1   Schematic diagram of experimental set-up for flame
            propagation experiments.

Figure 2   Schematic cross-sectional view of experimental chamber
            showing the obstacle configuration.

Figure 3   Schematic diagram of the flame propagation channel
            with obstacles.

Figure 4   Spark-schlieren photographs of stoichiometric methane-
            air flame propagation in a channel with obstacles.
            Obstacle height $H = 1.27$ cm; obstacle separation
            $P = 3.81$ cm.
            a) Channel width $W = 5.33$ cm. Dry ice in the second
               and fourth obstacles.
            b) Channel width $W = 5.08$ cm. No dry ice used.

Figure 5   Spark-schlieren photographs of stoichiometric methane-
            air flame propagation in a channel of width 2.54 cm
            with obstacles. Obstacle height $H = 1.27$ cm; obstacle
            separation $P = 3.81$ cm.
            a) Dry ice in the next to last obstacle.
            b) No dry ice used.

Figure 6   Schematic diagram illustrating flame propagation over
            obstacles.

Figure 7   Flame velocity $\dot{R}_f$ vs. distance of propagation r for
            stoichiometric methane-air flames. The solid curves
            correspond to Equation 7 with $\alpha = 0.31$ and $p_0 = 37.5$ cm.

a) Copper tube spiral; H = 1.25 cm, p = 3.75 cm on
   bottom plate, plastic tube spiral; H = 4 cm p = 10 cm
   on top plate; H/D = 0.52.

b) Copper tube spiral on bottom plate; H/D = 0.34.

c) Copper tube spiral on bottom plate; H/D = 0.25.

d) Copper tube spiral on bottom plate; H/D = 0.125.
   The experimental point at 30 cm is from the laboratory
   results of Reference 7.

Figure 8   Flame velocity $\dot{R}_f$ vs distance of propagation r for
stoichiometric methane-air flames. The solid curves
correspond to Equation 6 with α = 0.31 and p_0 = 37.5 cm.
Dashed curves are drawn through data points for x < 60 cm.

a) Plastic tube spirals; H = 4 cm, p = 10 cm, on both
   top and bottom plates; H/D = 0.67.

b) Plastic tube spiral on bottom plate; H/D = 0.57.

c) Plastic tube spirals; ') top plate only; '') top
   and bottom plate; H/D = 0.4.
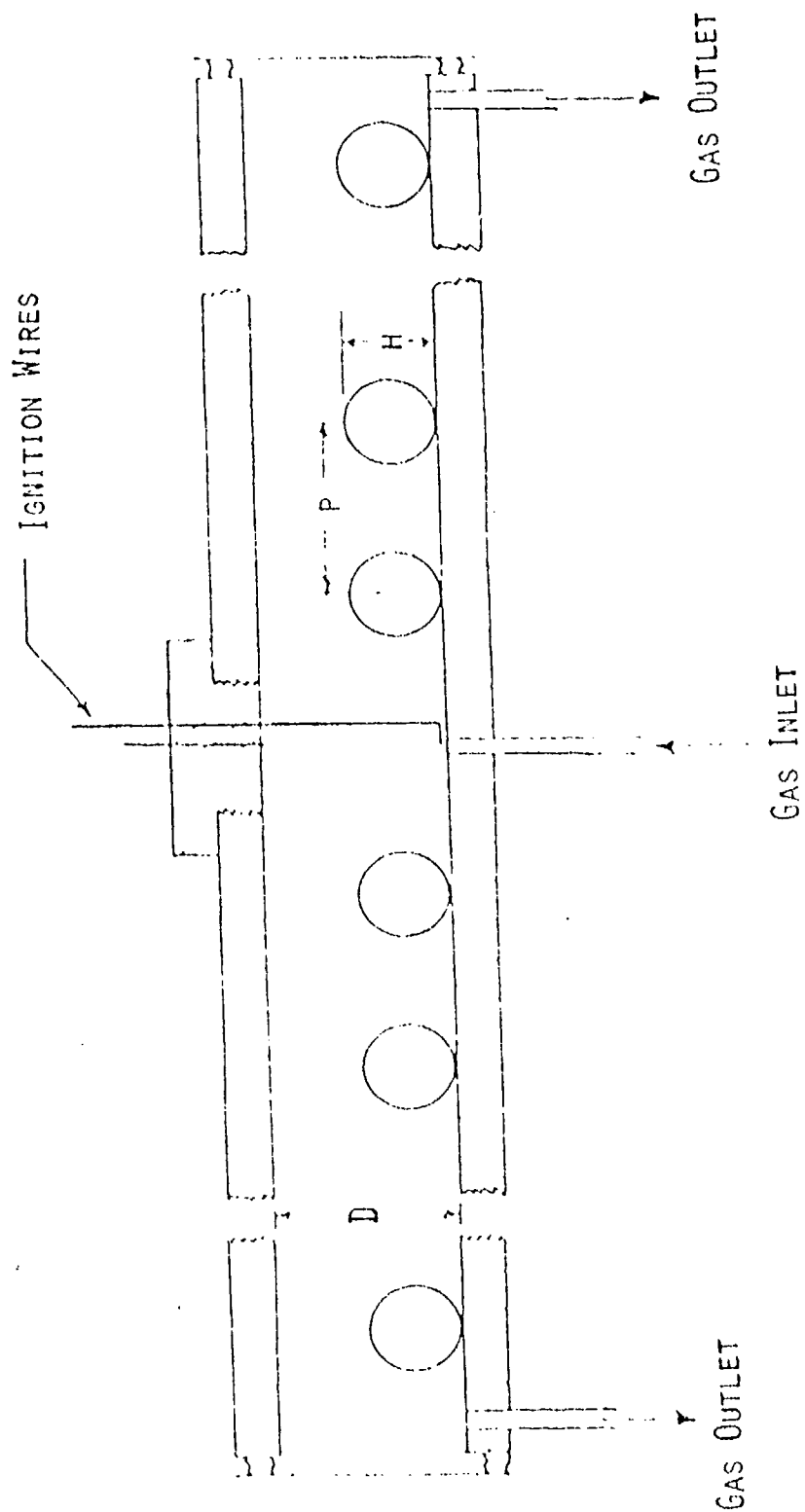
d) Plastic tube spiral on bottom plate; H/D = 0.33.

Gas Supply

Flow Meters

Ignition Wires
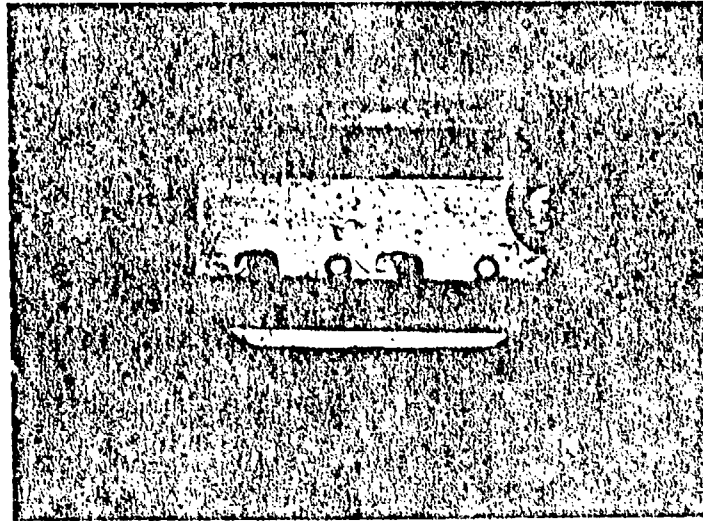
Gas Inlet

Spacer

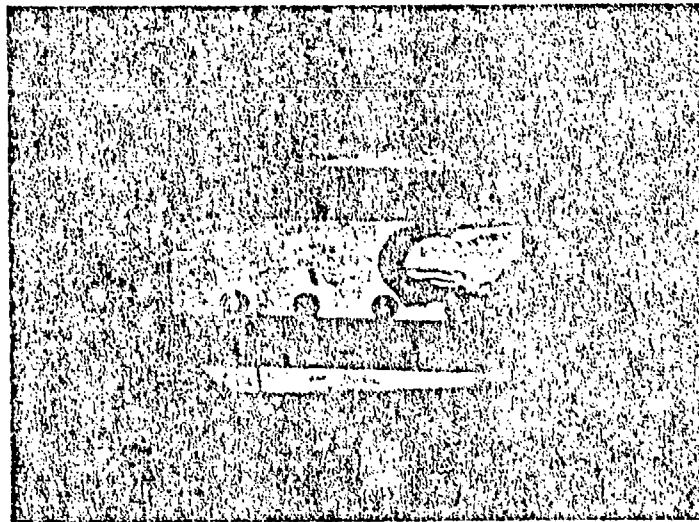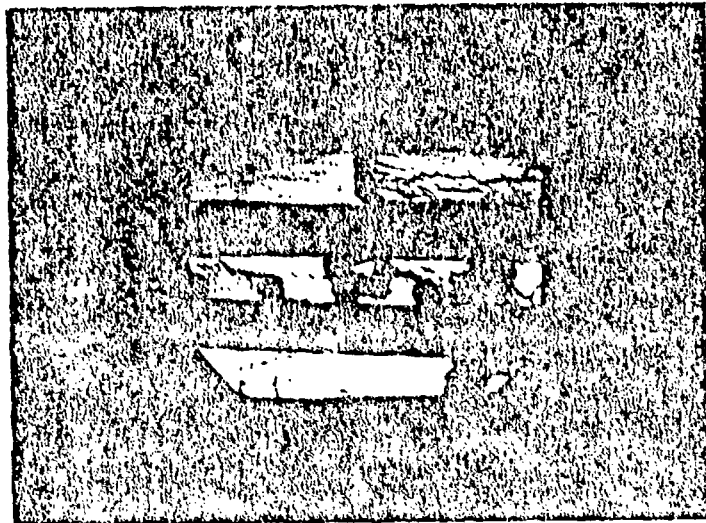Streak Camera
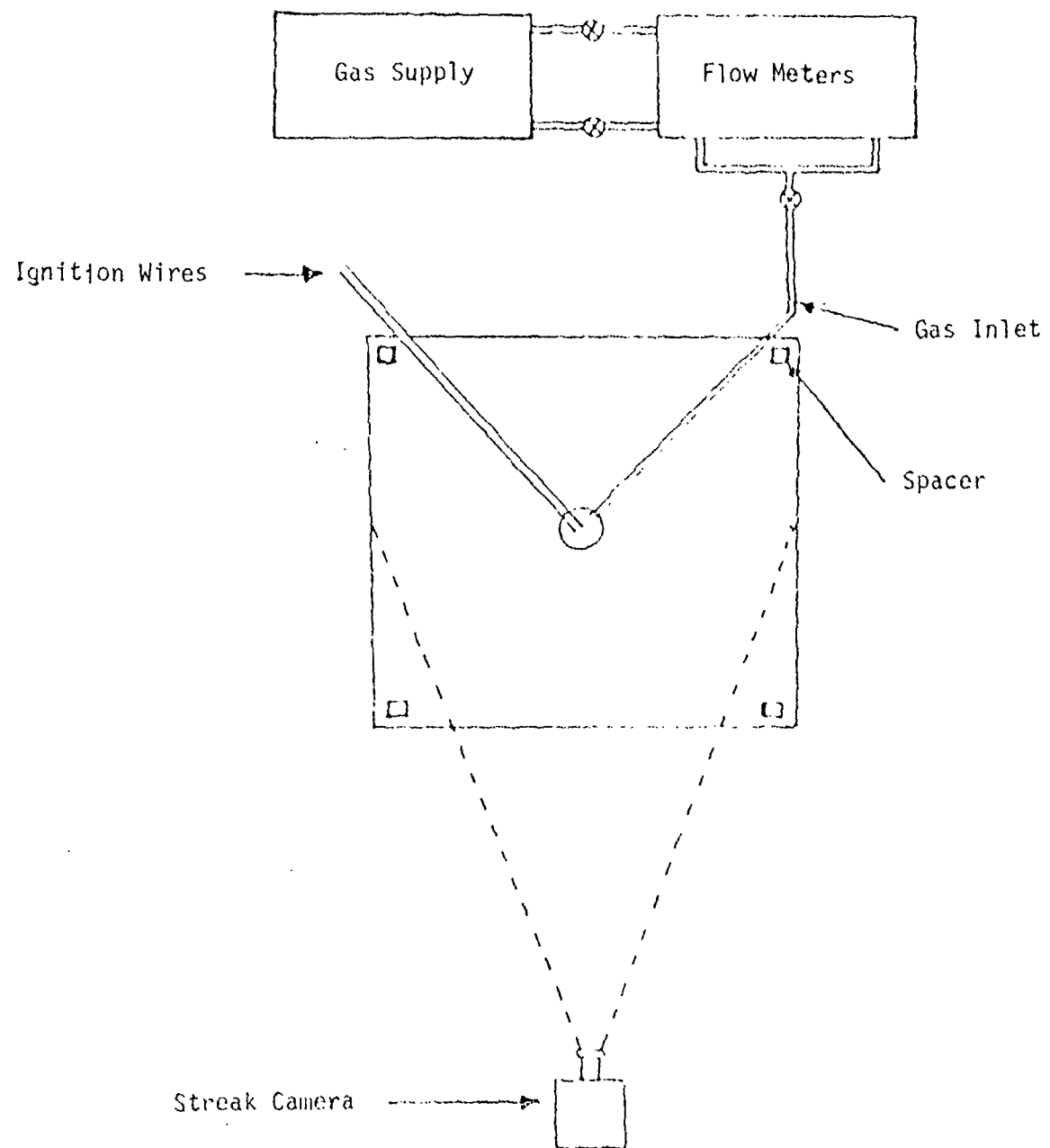
Figure 1

Figure 2

IGNITION SOURCE

30 cm.

H

P
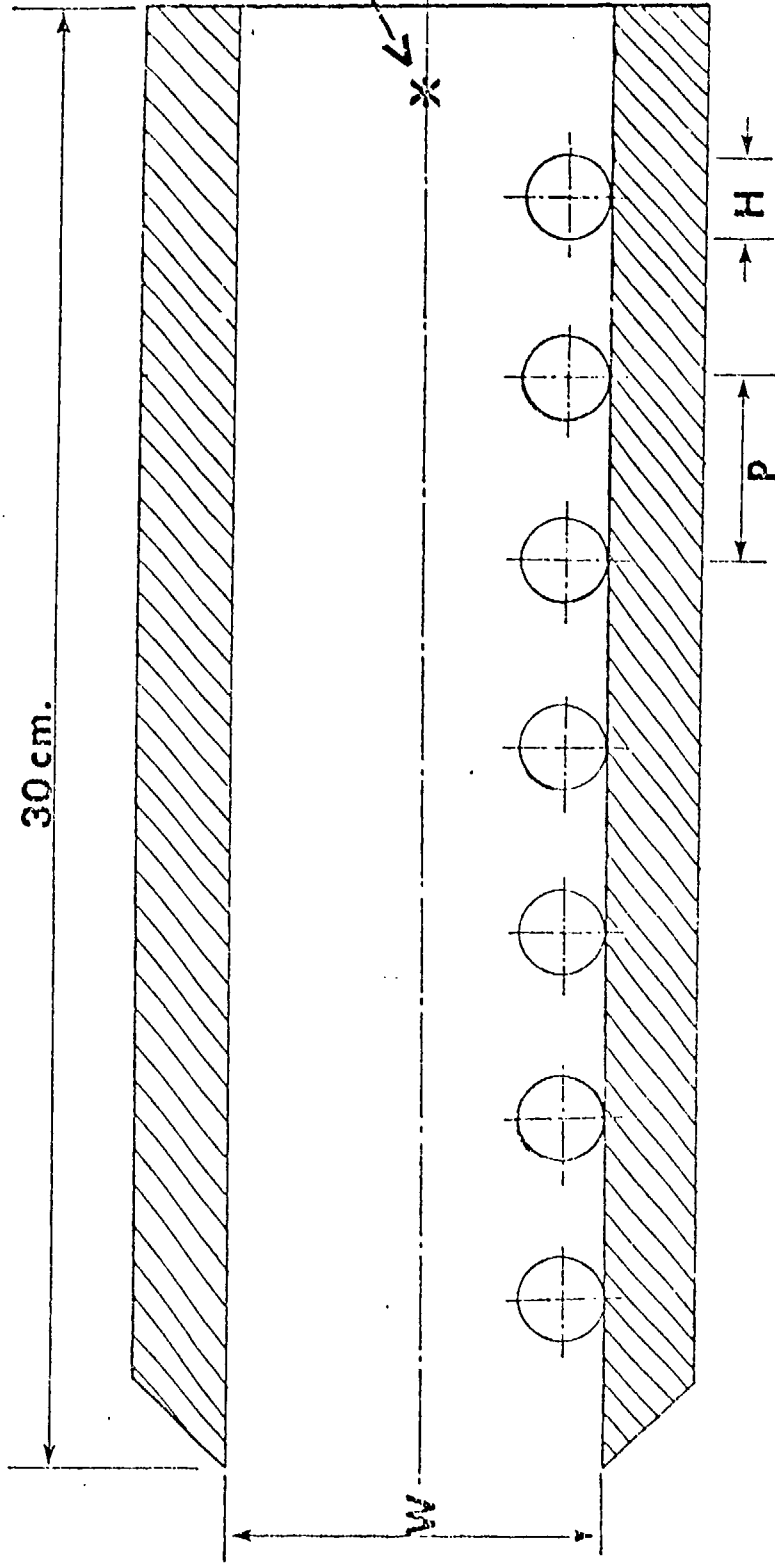
Figure 3

a)

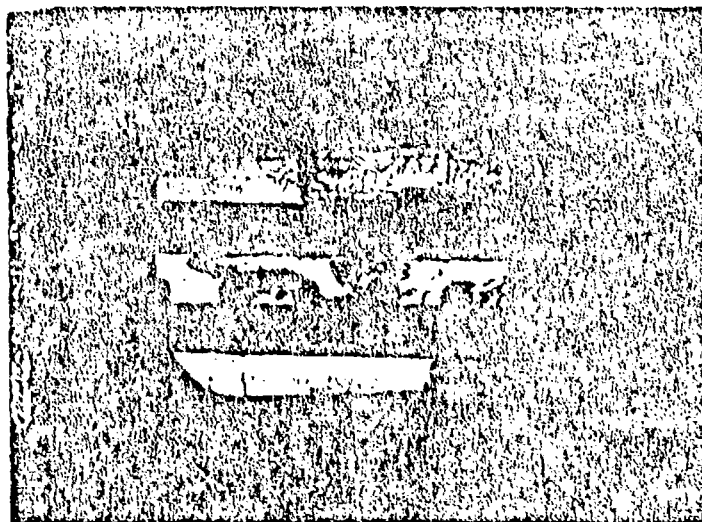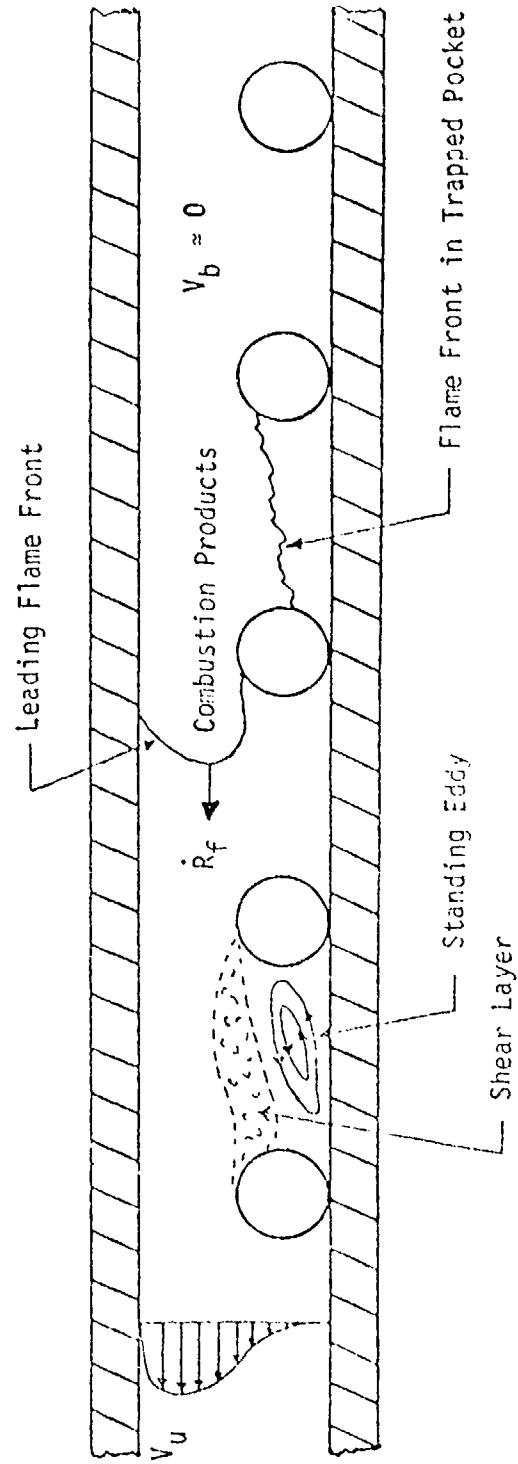
b)

Figure 4

a)

b)

Figure 5

Figure 6
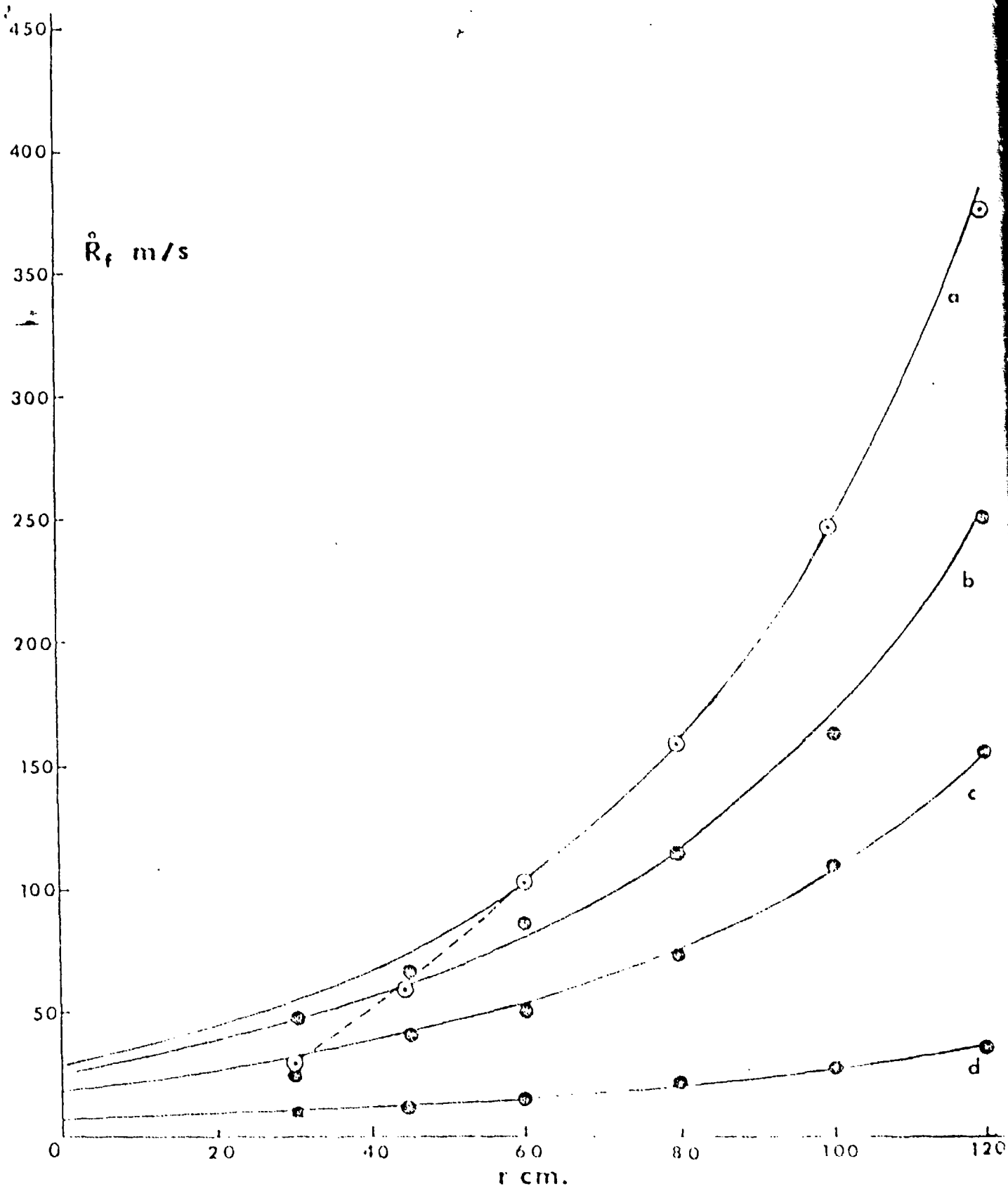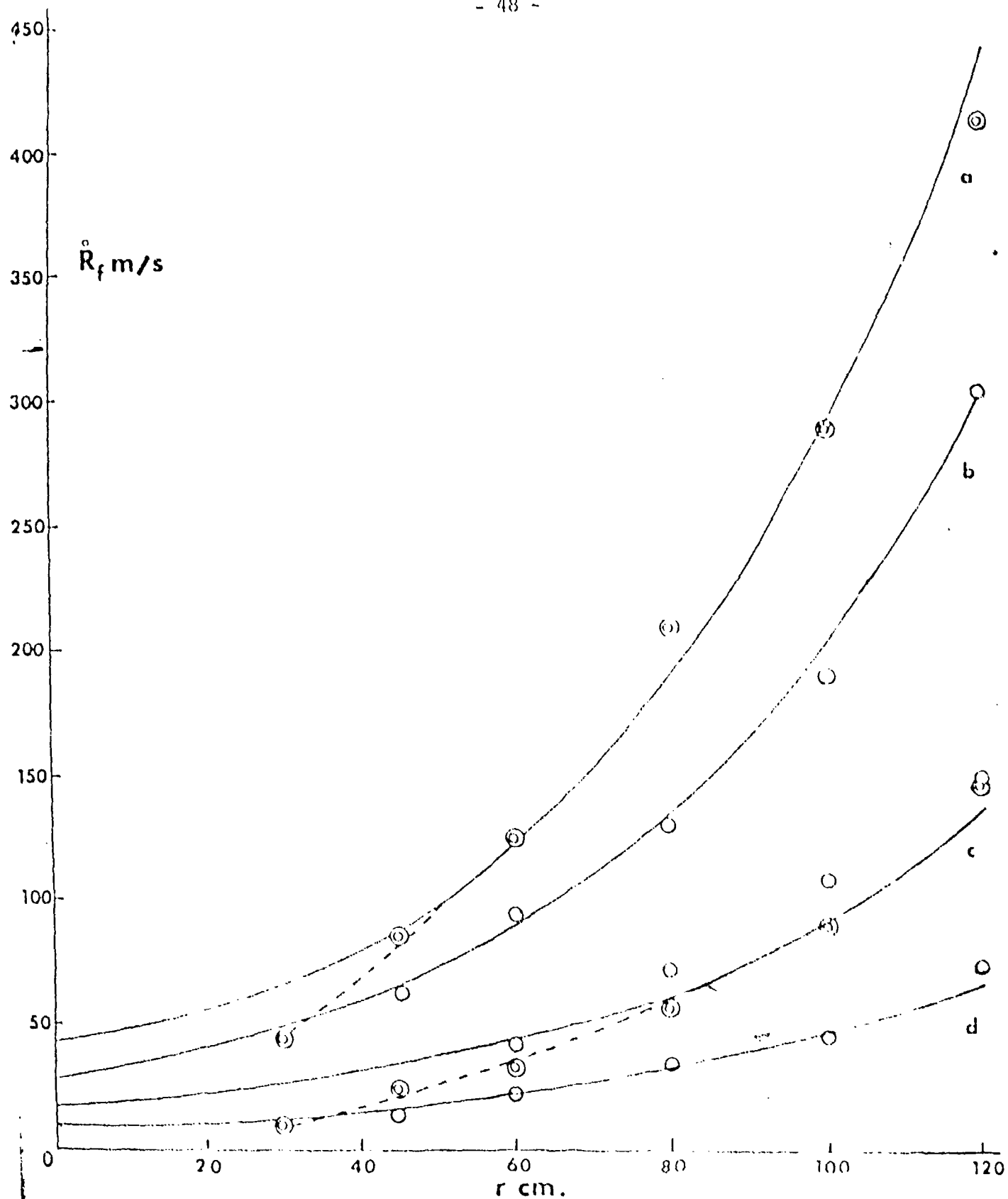
Figure 7

Figure 8

APPENDIX III

The Influence of Confinement on the Propagation of
Detonations near the Detonability Limits*

1. Introduction

One of the fundamental properties of an explosive gas mixture is the composition limits of detonability.. At the present time it is not possible to predict the detonability limits of a given mixture theoretically and the limits must be determined experimentally. Experiments to determine the detonability limits are usually performed in detonation tubes. Since a fairly strong initiation source (eg., a solid explosive charge or a volume of readily detonable mixture) is required for near limit mixtures, long tubes are required to ensure that the influence of the initiation source on the propagation of the detonation can be neglected at the observation section near the end of the tube. Just how long a tube is required for a given initiation source is not known. Furthermore, the influence of the tube itself (i.e., the tube diameter and the cross-sectional geometry) on the propagation of the detonation is not known. In fact, no generally accepted operational definition for the detonability limits based on experiments in finite length tubes has been established. Manson et al.[1] have suggested that the fluctuations of the local detonation velocity U_ℓ relative to average velocity U_m be used as criteria for the stability of the detonation in a tube. They suggest that self-sustained detonations for which U_ℓ and U_m agree within about $\pm 0.2\%$ can be considered as stable. However, this is an arbitrary definition. The appearance of near limit phenomena such as spin has also been suggested as a criteria for the limit in a given tube,[2] but it has not been established that the appearance of spin or other near limit phenomena in a given tube corresponds to a unique composition.

Further studies are clearly required in order to achieve a better understanding of the influence of the tube and the initiation on the near limit propagation of detonation waves in tubes before a meaningful operational definition of the limit can be deduced. This paper reports on the first

results of our investigation on near limit phenomena in tubes of different
diameter.

2. General Considerations

It is now well known that the classical theory of a detonation
which regards a detonation wave as a strictly one-dimensional structure con-
sisting of a shock wave followed by a reaction zone is an inadequate descrip-
tion of the detonation phenomena. Numerous detailed investigations of the
structure of detonations over the past 50 years have shown that the propaga-
tion of a detonation is a complex three-dimensional phenomena involving the
interactions of finite amplitude transverse waves with the leading shock front,
the reaction zone and the boundaries of the system. The kinematics of these
interactions have been explored in considerable detail by various investiga-
tors.[3,4,5] Although the three-dimensional transverse wave structure of deto-
nations is observed for unconfined detonations, the most detailed investiga-
tions of this structure have been done in confined rectangular or round deto-
nation tubes. In these cases, in particular for conditions marginal to the
propagation of the detonation wave (i.e., close to the detonability limits),
the influence of the tube walls cannot be neglected. The tube walls have
two different effects; namely, an energy and momentum loss associated with
the boundary layers and a stabilizing effect on the transverse wave structure.
For small diameter tubes the observed decrease in velocity with decreasing
tube diameter[6,7] can be understood in terms of the influence of the boundary
layers.[8,9] On the other hand, it is also observed that an apparently self-
sustained detonation in a confined tube fails once it emerges into an area

expansion or an unconfined region.[5,11,11] For a given mixture there appears to be a minimum critical tube diameter required in order for the detonation to continue to propagate under unconfined conditions. It has been suggested that this critical tube diameter is related to the characteristic transverse wave spacing of the detonation.[12,13] In other words, a minimum number of transverse waves is required for a self-sustained detonation in an unconfined situation, thus indicating that the pronounced three-dimensional structure observed in tubes near the detonability limits is stabilized by the confinement provided by the tube walls.

A possible relation between the spinning detonations observed in tubes and the detonability limits has been discussed by Dove and Wagner,[2] who suggested that the condition for stable propagation of a detonation wave in a tube is for the reaction time to be short enough to maintain the spin mode of the lowest frequency in the tube. Thus if the onset of the single-head spin structure corresponds to a unique fuel composition, the limit could be defined on this basis. Associated with this limit there would then be a characteristic chemical length scale which can be related to the tube diameter and geometry using the acoustic theory of spin detonations of Manson[14] and Fay.[15] The success of the acoustic theory in predicting the frequency or pitch of the transverse or spinning vibrations observed behind the detonation front further indicates that boundary conditions do play an important role for the propagation of detonations in confined tubes. In fact, according the the acoustic theory of Fay and Manson, the spin frequencies are entirely determined by the boundary conditions and do not depend on the details of the coupling between the gasdynamics and the chemical kinetics which gives rise to the transverse instability in the first place. The only condition being that the reaction time or chemical time be short enough to maintain the spinning mode, as discussed by Dove and Wagner.[2]

The mechanism by which the transverse waves are excited and maintained is not completely understood. However, the work by Barthel and Strehlow,[16] Erpenbeck,[17] Toong[18] and others has clearly shown that acoustic and non-linear perturbations can be amplified through the coupling with chemical energy release. The amplitudes and wavelengths of the perturbations required to trigger the various instablities are not known. However, it appears that detonations are unstable to perturbations over a fairly wide range of wavelengths. According to Toong[18] the acoustic kinetic interactions depend on the order and the enthalpy of the reaction, the activation energy and most important of all the ratio of the characteristic acoustic time to the chemical time. This is further supported by the work of Erpenbeck[17] who established the stability limits of detonations for various degrees of overdrive assuming a first order Arrhenius rate expression. Although the range of wavelengths over which the detonation is unstable depends on the activation energy and the degree of overdrive, he finds that detonations are stable only at short wavelengths (i.e., short compared to the length of the reaction zone), and also at long wavelengths for sufficiently large degrees of overdrive. From these investigations it appears that transverse waves with wavelengths over a fairly wide range can be excited. Thus the transverse wave structure of a detonation will depend on the preferred transverse mode (or modes). This preferred mode will be determined not only by the gasdynamic-chemical kinetic coupling, but also by the boundary conditions (for example, the geometry and diameter of the detonation tube). As long as the characteristic transverse dimensions associated with the boundary conditions are much larger than the characteristic wavelength associated with the chemical kinetics and gasdynamics, the boundary conditions will play a minor role in determining the transverse wave structure. However, for tube diameters of the order of the characteristic transverse wavelength or smaller, the boundary conditions will begin to play a more dominant role, so that for the same mixture the

detonation phenomena observed in a small diameter tube could be completely different to that which would be observed in an unconfined situation or in situations with different boundary conditions. Not only could the structure of the detonation wave be different, but composition limits of detonability could also vary with boundary conditions. In fact, it may be possible to trigger "detonation" phenomena in a tube outside of the limits of detonability for an unconfined situation. The phenomena of "galloping" detonations observed by Mooridan and Gordon,[19] Manson et al,[20] and Edwards and Morgan[21] may be an example of such a phenomena. If this is the case and if the onset of the "galloping" mode is sufficiently precise, then the onset of the "galloping" mode could also provide a criteria for determining the detonability limits. The "galloping" mode is a longitudinal mode with periodic destruction and reformation of the detonation and, as has been pointed out by Urtiev and Oppenheim,[22] the reformation process is identical to the transition form deflagration to detonation. "Galloping" detonations can therefore be considered to consist of periodic transitions, in which case the tube walls and confinement are known to play an important role. However, the role of the transverse waves, which are observed in near limit mixtures in maintaining the detonation wave is not understood.

We have undertaken a program to investigate the propagation of detonations in long tubes (14 m) of different diameters (5 cm up to 30 cm). The aim of the program is to determine a criteria for establishing the detonability limit in unconfined situations based on laboratory experiments and to investigate near limit phenomena to clarify the role of confinement on the propagation of detonations. This paper reports on the first part of this investigation which involved a detailed study of the propagation of detonations in ethylene-air mixtures near the lean limit in two long tubes (14 m) of diameter 5 and 15 cm. The transverse wave structure

of the detonations was observed by pressure transducers at various positions along the tubes as described in detail in the next section. A detailed discussion and interpretation of the results are given in Sec. 4 and Sec. 5 is the conclusion.

3. Experimental Details

The experimental apparatus consisted of two steel tubes of 4.8 cm and 14.5 cm in diameter with respective lengths of 14.15 m and 14.63 m. The ethylene-air gas mixture was prepared in continuous flow with the required flow rates of each component gas monitored via the pressure drop across capillary tubes.

The accuracy of the gas mixture produced was within 0.1% for the flow system associated with the 4.8 cm diameter tube and within 0.2% for the 14.5 cm tube. To ensure proper gas concentration in the experimental apparatus, the filling procedure consisted in first evacuating the tubes, then filling them with one atmosphere of the required gas mixture, followed by a further flowing of gas mixture through the tubes at one atmosphere for an equivalent of five fill times. All the experiments were done at one atmosphere.

The velocity and pressure records were obtained from P.C.B. Piezotronics transducers located at different positions along the tubes (Fig. 1). In the 4.8 cm tube the first two transducers were located at 2.3 m and 3.3 m from the ignition flange. Next a series of five transducers 0.5 m apart, with the first being used as a trigger, was located near the middle of the tube starting at a distance of 7.32 m from the ignition. Six more transducers were located near the end of the tube. The first transducer situated at 10.82 m was used as a trigger. The next transducer was connected to a Biomation digital recorder so that clear pressure traces could

be obtained. All other transducers were used in conjunction with standard oscilloscopes to obtain their respective pressure traces. Similarly for the 14.5 cm tube a total of nine transducers were used, with three located near the middle starting at a distance of 7.32 m and separated by a distance of 60.96 cm. The final six transducers were located near the end of the tube as indicated in Figure 1b.

The ignition system consisted of flowing a slug of oxy-acetylene gas mixture into the tube and igniting it with a high voltage capacitor spark. The gas mixture concentration was varied between equimolar and 20% C_2H_2 - 80% O_2, and slug lengths between three meters and half meter. A slug of half a meter was found to be the minimum length in which direct initiation of a detonation could be reliably obtained because of diffusion effects between the oxy-acetylene and the test gas mixture already in the tube. The characteristics of the ignitor were determined by detonating different concentrations and lengths of the ignitor slug into air. The shock velocities were measured at the end of the tube for the different ignitors and in all cases relatively weak shocks of similar strength (450-550 m/s) were observed.

Finally two spirals to be used in the 2.85 cm diameter tube were made from 0.32 cm copper tubing. The length of each was 1.5 m and the pitches were 15 cm and 1.6 cm. They could be positioned either near the beginning (1.535 m) or near the middle (6.81) of the tube.

4. Results and Discussion

The detonation velocities for different compositions of ethylene-air observed near the end of the tubes are compared with the theoretical C-J value in Fig. 2. The experimental points correspond to the average velocity measured from the set of transducers near the end of tubes. As can be seen from Fig. 2, the velocities measured in the 4.8 cm diameter

tube are in good agreement with the theoretical values over the whole range of compositions from 6% to 3% ethylene in C_2H_4-air. However, in the larger 14.5 cm diameter tube the observed velocities begin to consistently deviate significantly from the theoretical value below 5% C_2H_4 in C_2H_4-air. At 3.5%, for example, the observed average velocity is approximately 13% lower than the theoretical value. As will be discussed later, this region also corresponds to the region where the pressure structure of the detonations in the two tubes differs significantly.

These results are for "self-sustained" detonations which are directly initiated by the detonation of the acetylene-oxygen charge (super-critical initiation) and whose observed velocity is constant over the last half of the tubes within experimental errors ($\pm$ 3%). If the initiation charge is not strong enough to produce a detonation initially (i.e., sub-critical initiation) so that a decoupled shock flame complex is observed at the first two transducers in the 4.8 cm diameter tube, or if obstacles in the form of Shchelkin spirals are placed in the 4.8 cm diameter tube, com-pletely different phenomena are observed. In these cases large fluctuations in velocities are observed for mixtures which exhibit strong single head spin structure for super-critical initiation. The phenomena is analogous to the "galloping" detonations observed by Mooridan and Gordon,[19] Manson et al,[20] and Edwards and Morgan.[21] The wave appears to propagate in a cyclic manner exhibiting large velocity fluctuations with velocities ranging from 2100 m/s down to about 900 m/s. This phenomena of cyclic propagation is observed for subcritical initiation for 3.5% C_2H_4 and below. Unfortunately, with our pre-sent ignitor system, subcritical initiation above 3.5% C_2H_4 could not be achieved in a reliable manner, so that it cannot be concluded that similar propagation phenomena are not possible in richer mixtures. When Shchelkin spirals placed near the beginning of the tube were used to dissociate the

detonation wave, the observed transition near the end of the tube is the same as that of a galloping cycle, and for fuel compositions below about 4.5% C_2H_4 the original spinning detonation is not re-established by the end of the tube. Thus, although apparently stable detonations are observed in the 4.8 cm diameter tube all the way down to 3% C_2H_4 in C_2H_4-air, the detonations which exhibit clear single head spin are very sensitive to both the initial conditions and to the boundary conditions. By changing the initiation energy or by placing obstacles in the tube completely different modes of propagation are observed. Also, detonations in the same near-limit fuel mixture but in the two different diameter tubes have significantly different structure, c ' ': the propagation velocity appears to be constant in both tubes.

For mixture compositions far removed from the detonability limit the pressure records show a typical multi-headed detonation in both the small (4.8 cm diameter) and the large (14.5 cm diameter) tube. Examples of such pressure records are shown in Fig. 3. Even for these compositions, there are distinct pressure variations of the order of 5-10 atm near the front resulting from the three dimensional structure of the detonations. However, the frequencies of these variations ($\sim$100 Kc/s) are an order of magnitude larger than the characteristic lowest mode spin frequency ($\sim$10 Kc/s) and the pressure vibrations disappear within two or three cycles. Thus for these mixtures the characteristic chemical gasdynamic transverse wavelength is an order of magnitude smaller than the dimensions of the tube and there is apparently no strong coupling of the detonation to the boundary conditions. This should be contrasted with the structure observed for near-limit mixtures. Fig. 4 shows typical examples of pressure records observed for 3.3% C_2H_4. Notice that the structure of the detonation in the small tube (Fig. 4a) differs markedly from that observed in the large tube (Fig. 4b). Both pressure

traces show the characteristic pressure variations due to a single-head spin-
ning wave behind the detonation front, but since the diameter of the tubes
are different the spin frequencies are different. In the small tube the
characteristic time of the pressure oscillations behind the front $\delta t \simeq 0.1$ ms
corresponding to spin pitch $P = \delta t U$ (where U is the wave velocity) of about
15 cm and a spin pitch to tube diameter ratio $P/D = 3.1$. Similarly, in the
large tube the characteristic time $\delta t \simeq 0.27$ ms corresponding to a P/D ratio
of about 2.5. The pressure pulses observed in Fig. 4 correspond to pressure
variations of the order of 10 atm and are clearly not acoustic pulses, never-
theless it is useful to compare the observed ratio of P/D to that obtained by
considering the pulses to be due to an acoustic spinning wave. For a purely
transverse acoustic wave we have[15] $P/D = \frac{\pi}{k_n} (\frac{U}{c})$, where c is local speed of
sound and k_n is the root of the first derivative of the Bessel function of
order n ($k_1 = 1.841$ and $k_2 = 3.054$). The theoretical value at 3.3% C_2H_4 is
$P/D = 2.97$ which is in good agreement with the pitch to diameter ratios ob-
served, especially in view of the approximations involved (i.e., acoustic
waves, C-J values for U and c). From these observations it is clear that for
this composition the spin pitch or spin frequency is determined by the cha-
racteristic dimensions of the tubes rather than by some characteristic length
associated with the rate of chemical reaction. This conclusion is further
supported by the observations that in the small tube the same spin pitch to
diameter ratio is observed over the range of compositions from 4.2% to 3%
C_2H_4, indicating that for these compositions the confinement or boundary con-
ditions determine the transverse modes which dominate the propagation of the
detonation. Similarly, in the large tube transverse modes characteristic of
the tube rather than the mixture dominate the propagation between about 3.5
and 3% C_2H_4. At 3% C_2H_4 some of the single head spin detonations that ap-
peared to be stable over the first half of the tubes (i.e., for about 7 m)
were observed to decay completely by the end of the tube. Thus as the

characteristic spinning mode associated with the tube gets further and further out of tune with the characteristic chemical time, or equivalently as stated by Dove and Wagner,[2] the chemical reaction time gets too long to maintain the spin mode, the detonation becomes unstable. Below 3% C_2H_4 we were unable to maintain any form of detonation modes in either of the tubes.

As mentioned previously the single head spin mode of propagation is also very sensitive to the initial conditions, indicating that the coupling between the gasdynamics, the chemical energy release and the boundary conditions must be properly established for a steady state detonation to propagate the length of the tube. If this coupling is not established from the beginning a "galloping" mode of propagation is observed. This phenomena appears to be controlled by the amplification of transverse waves in the reaction zone behind a leading shock front. Pressure records of the different phases of the propagation for 3.3% C_2H_4 in the 4.8 cm diameter tube are shown in Fig. 5. Fig. 5a shows a fairly weak shock wave ($\Delta p \approx 6$ atm) followed by a reaction zone with intense pressure oscillations in excess of 30 atm peak to peak with a frequency of the order of the spin frequency. The second trace which is taken 50 cm downstream of the first trace shows the amplification of the pressure oscillations and the catching-up of the reaction zone to the leading shock wave. The velocity of the leading shock wave is 966 m/s or about 63% of the theoretical C-J velocity. The stage at which the transverse oscillations have just caught up to the leading front is shown in Fig. 5b. This leads to an overdriven detonation with a velocity of 2087 m/s which then decays to 1687 m/s between the last two pressure transducers. (Both the two top and two bottom traces are taken 50 cm apart, and the two middle traces are taken 1 m apart). A pressure trace taken 50 cm prior to the first trace of this figure shows a weak shock front (≈ 7 atm) followed by intense pressure variations at a time interval of 0.25 ms behind

the leading front. Notice that the transverse wave is absent in the over-driven state. It is not clear why it has dissapeared so quickly, however the effective reaction zone would now be much smaller and the low frequency mode would be incapable of being further exited. This is supported by Erpenbeck's[17] calculation showing that overdriven detonations are stable to a wider range of wavelengths than C-J detonations.

The overdriven or fast mode of propagation is further illustrated in Fig. 6a. In this case the velocity between the two top traces (separated by 50 cm) is 2050 m/s, and the wave decays to 1650 m/s between the last two traces (separated by 1.5 m). Notice that the characteristic pressure oscil-lations begin to reappear as the velocity approaches the C-J value of about 10 m/s, lending support to our previous argument for the absence of trans-verse wave in the overdriven state based on Erpenbeck's[17] analysis. The pressure trace shown in Fig. 6b is taken at a position between the bottom two traces of Fig. 6a. This trace shows that the wave actually consists of a relatively strong shock front ($\Delta p = 11.2$ atm) followed by a high pressure region ($\Delta p \simeq 20$ atm).

These results clearly show that transverse waves which are coupled to the tube are amplified in the chemical reaction zone behind the leading shock wave and a mode of unsteady propagation, consisting of transverse wave amplification with subsequent catch-up of the transverse wave region to the shock, resulting in an overdriven detonation which then decays and leads to a separation of the shock wave and the reaction zone. The process then re-peats itself. Transverse wave structure in the shock flame region during the dissociated or slow phase of galloping were also observed by Manson et al,[20] but their role in the unsteady propagation was not recognized. The explosion which occurs as the transverse wave catches up to the leading shock wave is similar to that which can also occur in flame to detonation

transition as Urtiew and Oppenheim[22] have pointed out.

To further clarify the role of the transverse waves for the propagation of detonations in tubes we inserted Shchelkin spirals at various positions in the small tube. Two spirals of different pitch were used, one of pitch 15 cm which corresponds approximately to the spin pitch observed in this tube. It was found that this spiral had almost no influence on the propagation observed at the end of the tube. However, for the spiral of pitch 1.6 cm the effect is quite dramatic. As shown in Fig. 7a this spiral completely destroys the transverse wave structure and the spinning detonation is completely dissociated as it leaves the spiral region as shown on the bottom trace. When this spiral is placed near the beginning of the tube, reformation due to the build-up of transverse waves occurs for composition above 3.5% C_2H_4. A typical record shows the transition about 7 m downstream of the spiral region for 4% C_2H_4 is shown in Fig. 7b. This transition is virtually identical to one phase of the galloping propagation observed with sub-critical initiation in 3.3% C_2H_4 shown in Fig. 7c. Notice that in both cases (i.e., Fig. 7b and 7c) the transverse vibrations in the reaction zone amplify and finally merge with the leading shock wave. In both cases, higher frequency modes are excited behind the leading shock wave and the velocities of the leading shock waves are between 900 and 1200 m/s (i.e., less than the C-J detonation velocity) during the merging process.

The near limit detonation phenomena observed in confined tubes are clearly strongly influenced by the spin vibrations associated with the characteristic modes of the tube. In fact, for mixtures whose characteristic gasdynamic-chemical transverse wavelength is less than or of the order of the transverse dimensions of the tube, completely different modes of propagation are observed depending on the coupling between the gasdynamics, chemical energy release and the walls of the tube. Due to the strong

influence of the confinement, both single head spin and galloping detona-
tions are observed over a fairly wide range of mixture compositions. These
near limit phenomena depend more on the tube than on the chemical kinetics
of the mixture. For different size or geometry tubes these near limit
phenomena would therefore be expected to occur at different mixture compo-
sitions. Thus detonability limits which are to be extrapolated to infinite
tube diameter or to the unconfined situation must exclude these phenomena.
We therefore propose that these detonability limits be characterized by the
composition at which clear single-head spin first appears in the tube.
At this composition the characteristic gasdynamic-chemical transverse wave-
length is approximately tuned to the size of the tube. This does not answer
the question of the number of transverse waves required for an unconfined
detonation, but it does provide a length scale for a given mixture composi-
tion, i.e., the tube diameter or the pitch of the spin, which can be used
to estimate the characteristic wavelength in an unconfined situation for
this mixture composition.

If we use the above criterion, we find that the lean detonability
limit for ethylene-air mixtures lies between 4.5 and 4.2% C_2H_4 in the 4.8 cm
diameter tube and between 4 and 3.5% C_2H_4 in the 14.5 cm diameter tube. The cha-
racteristic transverse wavelength of the mixture has therefore increased by a factor of
about 3 for a compositional change of about 0.7% C_2H_4. Typical pressure re-
cords showing the appearance of single head spin between these compositions
are shown in Fig. 8. Fig. 8a and b are pressure records of detonations in
the 4.8 cm diameter tube at 4.5% and 4.2% C_2H_4, respectively (note the dif-
ference in vertical scale). At 4.5% the characteristic time of the pressure
oscillations is of the order of 50 μsec (with still higher frequencies ob-
served near the front). A time of 50 μsec gives a spin pitch of about 8.35
cm and a pitch to diameter ratio of about 1.72. This therefore corresponds

to the second lowest spin mode whose pitch to diameter ratio calculated from acoustic theory is 1.81. At 4.2%, the characteristic time is about 90 μs (although there is some slight variation in frequency near the front) giving a pitch to diameter ratio of about 3, which corresponds to the lowest spin mode in this tube. Fig. 8c and d are the pressure records at 4% and 3.5% C_2H_4 in the 14.5 cm tube, respectively (note the different in vertical scale). The pressure oscillations near the front at 4% are separated by a time of about 0.1 ms to 0.15 ms, which is about half of the characteristic time associated with the lowest spin mode in this tube, indicating that a higher mode has been excited, at least near the front. This can be compared with the pressure oscillations at 3.5% which show no indication of any mode other than the lowest spin mode whose characteristic time is about 0.28 ms, corresponding to a pitch to diameter ratio of about 2.8.

The variation in characteristic wavelength with composition is expected to be very dramatic near the detonability limits and it is expected that for sufficiently large diameter tubes, single head spin would not be possible. The critical tube diameter above which single head spin is not observed would then correspond to maximum transverse wavelength possible for the mixture, and the composition corresponding to this characteristic wavelength would be the composition limit beyond which a detonation cannot be initiated no matter how large a volume of mixture is available. Clearly experimental investigations in different diameter tubes are required before any extrapolation can be attempted. These investigations are now in progress.

5. Conclusion

The propagation of detonations in confined tubes is clearly influenced by the confinement provided by the tube walls. This influence becomes particularly dramatic for marginal detonation waves with characteristic

transverse wavelengths of the order of or less than the tube diameter. In these cases single head spinning detonations whose pitch is determined by the diameter of the tube are observed over a fairly wide range of compositions. The structure of detonation therefore depends critically on the tube diameter and is maintained by the interaction of a combustion zone instability which couples to the characteristic modes of the tube. Thus for different diameter tubes, different characteristic transverse wavelengths are observed for the same mixture composition. Since these spinning modes, which are strongly coupled to the tube dimensions, would not occur at the same composition under unconfined conditions or in tubes of larger diameter we have proposed that the equivalent unconfined detonability limits be characterized by the composition at which single head spin is first observed in the tube. This then provides a length scale associated with the detonability limit which can be extrapolated to different situations. Based on this criteria we obtain a detonability limit between 4.5-4.2% ethylene in C_2H_4-air in a 4.8 cm tube and a limit between 4-3.5% in a 14.8 cm tube. Although this is clearly insufficient for any extrapolation it does provide a basis for further work in different size tubes which is now in progress.

The role of transverse spinning waves in maintaining a detonation-like phenomena in a round tube have been further clarified by varying the initiation energy and by inserting Shchelkin spirals at various positions along the 4.8 cm diameter tube. It is found that waves which exhibit apparently stable single head for the length of the tube for super-critical initiation propagate in an unsteady cyclic fashion analogous to galloping detonations for sub-critical initiation. The propagation of these unsteady waves is controlled by the amplification of transverse vibrations in the reacting zone behind the leading shock wave. As the transverse vibrations amplify they catch up to the shock wave leading to an overdriven detonation.

In this overdrive stage the transverse vibrations disappear and only begin to appear again as the velocity approaches the C-J value. The process then repeats itself. A similar phenomena is observed with the Shchelkin spiral in the tube. In this case the spiral destroys the transverse wave structure and the wave dissociates, transverse waves then amplify in the reaction zone region and transition occurs when these waves catch up to the leading flame front.

At this stage of our investigation the results are qualitative in nature but our detailed observations on the role of transverse vibrations in maintaining detonation-like phenomena in confined tubes suggests a new approach for further experimental and theoretical investigations. These investigations are now in progress.

References

1. Manson, N., Brochet, C., Brossard, J. and Pujol, Y., 9th Symposium (International) on Combustion, Academic Press Inc., New York, N.Y., 1963, p. 461.

2. Dove, J.E. and Wagner, H.Gg., 8th Symposium (International) on Combustion, Willams and Wilkins, 1962, p. 589.

3. Strehlow, R., Comb. and Falme, 1968, Vol. 12, p. 81.

4. Edwards, D.H., 12th Symposium (International) on Combustion, The Combustion Institute, Pittsburgh, Pa., 1969, p. 819.

5. Wagner, H.G., 9th Symposium (International) on Combustion, Academic Press Inc., New York, N.Y., 1963, p. 454.

6. Guenoche, H. and Manson, N., 6th Symposium (International) on Combustion, Reinhold, New York, 1957, p. 631.

7. Kistiakowsky, G.B. and Zinman, W.G., J. Chem. Phys., 1955, Vol. 23, p. 1889.

8. Zeldovich, Y.B., Zhur. Ekspth. i Teoret. Fiz., 1940, V. 10, p. 542.; translated in NACA Techn. Mem., 1950, p. 1261.

9. Fay, J.A., The Physics of Fluids, 1959, Vol. 2, p. 283.

10. Matsui, H. and Lee, J.H., 17th Symposium (International) on Combustion, The Combustion Institute, 1979, p. 1269.

11. Dabora, E.K., Nicholls, J.A. and Morrison, R.B., 10th Symposium (International) on Combustion, The Combustion Institute, 1965, p. 817.

12. Urtiew, P.A. and Traver, C.M., "Effects of Cellular Structure on the Behavior of Gaseous Detonation Waves under Transient Conditions", paper presented at the VIIth International Colloquium on Gasdynamics of Explosions and Reactive Systems, Göttingen, West Germany, 20-24 August 1979.

13. Edwards, D.H., Nettleton, M.A. and Thomas, G.O., J. Fluid Mech., 1979, Vol. 95, p. 79.

14. Manson, N., Compt. rend., 1946, Vol. 222, p. 46.

15. Fay, J.A., J. Chem. Phys., 1952, Vol. 20, p. 942.

16. Barthel, H.O. and Strehlow, R.A., Physics of Fluids, 1966, Vol. 9, p. 186.

17. Erpenbeck, J.J., 12th Symposium (International) on Combustion, The Combustion Institute, Pittsburgh, 1969, p. 771.

18. Toong, T.-Y., Acta Astronautica, 1973, Vol. 1, p. 317.

19. Mooradian, A.J. and Gordon, W.E., J. Chem. Phys., 1961, Vol. 19, p. 1116.

20. Saint-Cloud, J.P., Guerraud, C., Brochet, C. and Manson, N., Astronautica Acta, 1972, Vol. 17, p. 487.

21. Edwards, D.H. and Morgan, J.M., J. Phys., 1977, Vol. D10, p. 2377.

22. Urtiew, P.A. and Oppenheim, A.K., Proc. Roy. Soc., 1968, Vol. A304, p. 379.

Figure Captions

Fig. 1   Schematic diagram of the experimental apparatus.

      a) 4.8 cm diameter tube,

      b) 14.5 cm diameter tube.

Fig. 2   Comparison of average detonation velocities measured at

      the end transducers in the two detonation tubes with

      theoretical Chapman-Jouguet detonation velocities for

      different fuel compositions.

Fig. 3   Typical pressure records of multi-head detonations in

      ethylene-air mixtures.

      a) 5% C_2H_4 in 4.8 cm diameter tube. Biomation record:

       Time base: 20 µsec/div.

       Vertical scale: 6.8 atm/div.

      b) 7.8% C_2H_4 in 14.5 cm diameter tube. Biomation record:

       Time base: 20 µsec/div.

       Vertical scale: 6.8 atm/div.

Fig. 4   Pressure records showing single-head spin detonations in

      ethylene-air mixtures.

      a) 3.3% C_2H_4 in 4.8 cm diameter tube. Biomation record:

       Time base: 100 µs/div.

       Vertical scale: 6.8 atm/div.

      b) 3.3% C_2H_4 in 4.8 cm diameter tube. Biomation record:

   Time base: 100 µs/div.

   Vertical scale: 6.8 atm/div.

Fig. 5   Pressure records of near limit phenomena observed in the

      4.8 cm diameter tube for sub-critical initiation of 3.3%

      C_2H_4.

a) Amplification of the spinning wave behind the shock
front at the end transducers.
Time base: 0.2 ms/div.
Vertical scale: 13.6 atm/div.

b) The transition process observed at the end transducers.
Time base: 0.2 ms/div.
Vertical scale: 13.6 atm/div.

Fig. 6   Pressure records showing the fast phase of the propagation
of galloping detonation for sub-critical initiation at
3.3 C_2H_4 in the 4.8 cm diameter tube.

a) Top three traces are taken 0.5 m apart and the bottom
two traces are taken 1.5 m apart (at the end transducers)
Time base: 0.5 ms/div.
Vertical scale: 13.6 atm/div.

b) Biomation record taken between two bottom traces in Fig. 6a.
Time base: 20 μsec/div.
Vertical scale: 3.4 atm/div.

Fig. 7   a) Pressure records taken in the region of spiral obstacles
of pitch 1.6 cm in the middle of the 4.8 cm diameter tube
showing the dissociation of the spinning wave by the
obstacles at 3.5% C_2H_4.
Time base: 0.5 ms/div.
Vertical scale: 11.3 atm/div.

b) Pressure records showing the transition process 7m
downstream of spiral obstacles of pitch 1.6 cm for 4%
C_2H_4 in 4.8 cm diameter tube.
Time base: 0.2 ms/div.
Vertical scale: 11.3 atm/div.

c) Pressure records taken at the middle transducers for
sub-critical initiation of 3.3% C_2H_4 in the 4.8 cm tube.
Time base: 0.2 ms/div.
Vertical scale: 11.3 atm/div.

Fig. 8   Pressure records showing the onset of single head spin in
ethylene-air mixtures.

a) 4.5% C_2H_4 in 4.8 cm diameter tube. Biomation record:
Time base: 0.1 ms/div.
Vertical scale: 3.4 atm/div.

b) 4.2% C_2H_4 in 4.8 cm diameter tube. Biomation record:
Time base: 0.1 ms/div.
Vertical scale: 6.8 atm/div.

c) 4% C_2H_4 in 14.5 cm diameter tube. Biomation record:
Time base: 0.1 ms/div.
Vertical scale: 2.7 atm/div.

d) 3.5% C_2H_4 in 14.5 cm diameter tube. Biomation record:
Time base: 0.1 ms/div.
Vertical scale: 6.8 atm/div.

Fig. 1

Fig. 2

O 4.8 cm diameter tube

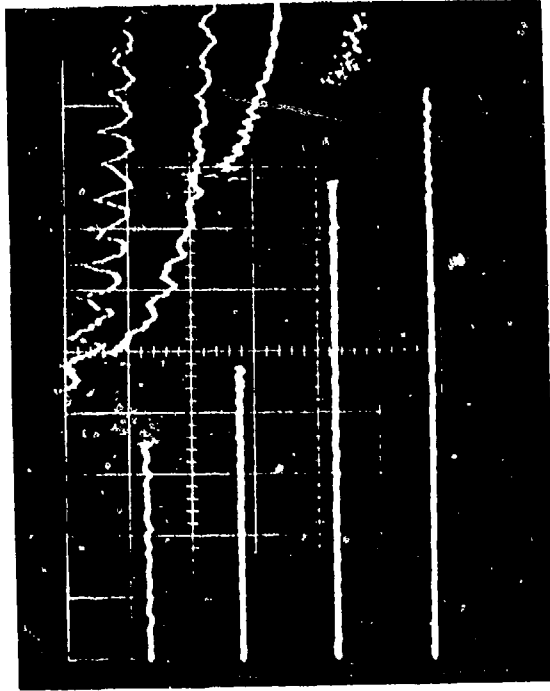□ 14.5 cm diameter tube

% C₂H₄ by Volume in C₂H₄-Air

V_CJ m/s
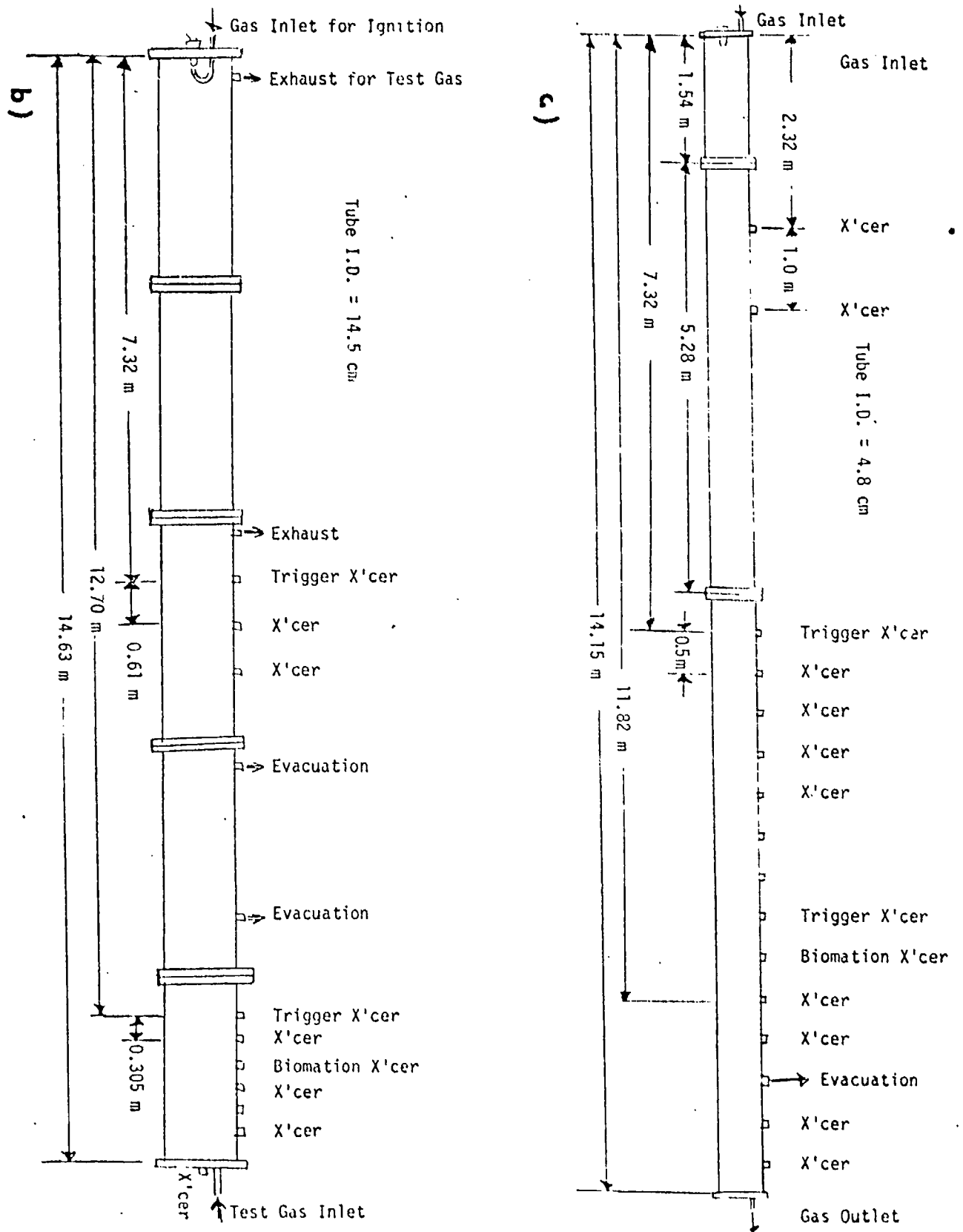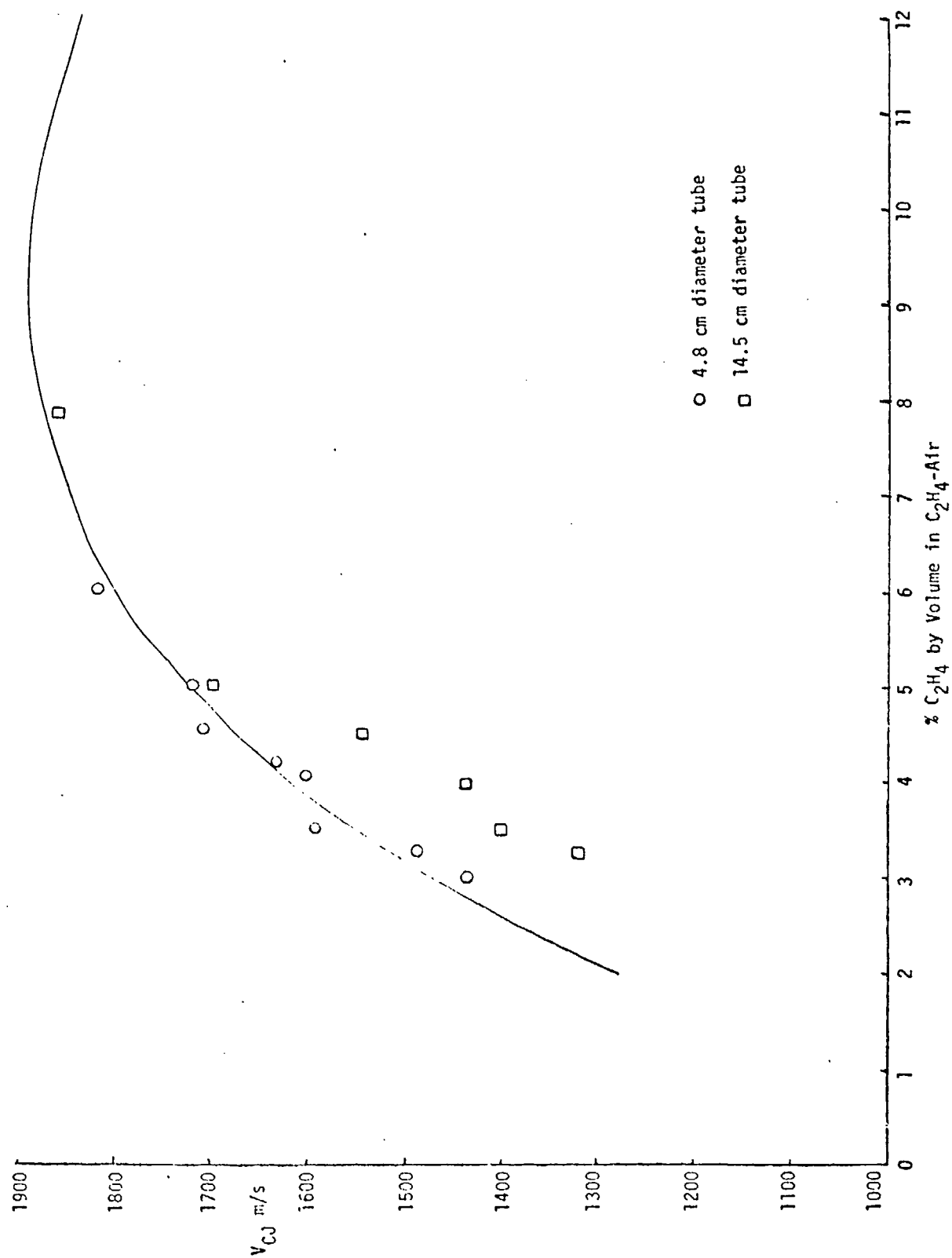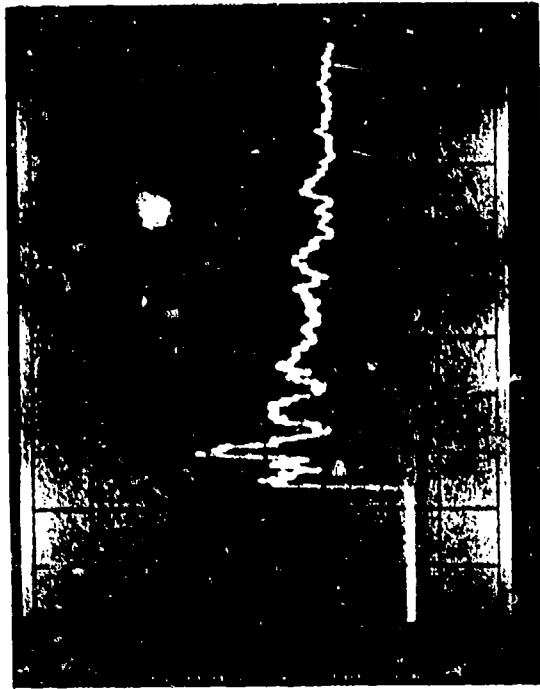
Fig. 3b

Fig. 4b
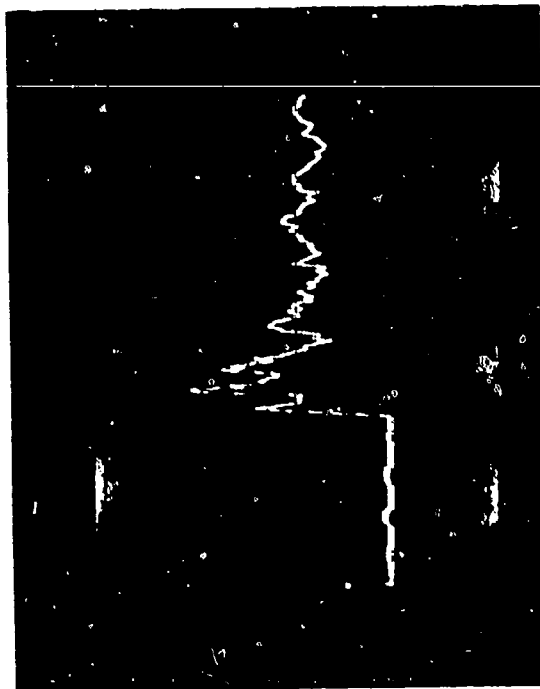
Fig. 3a

Fig. 4a

Fig. 5b

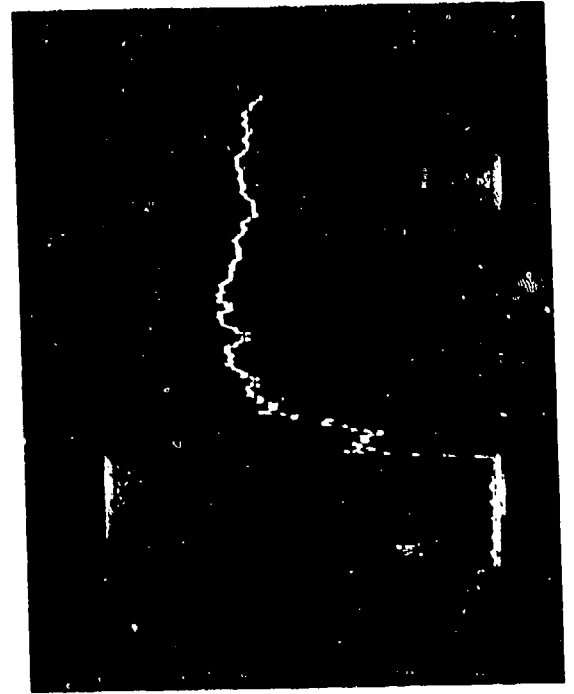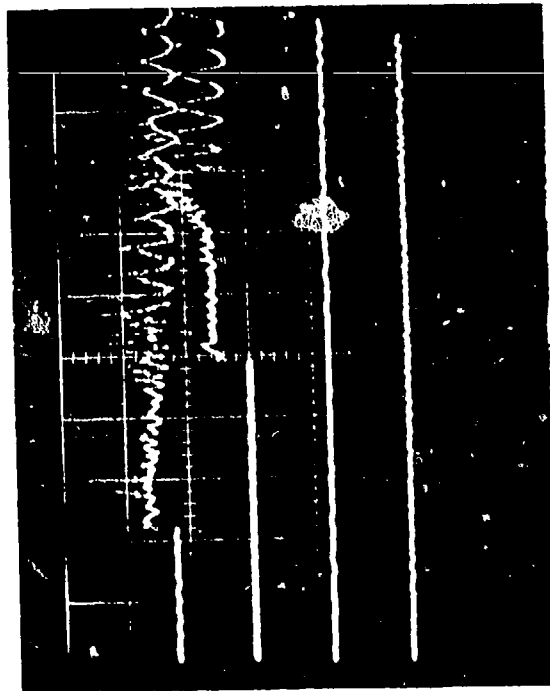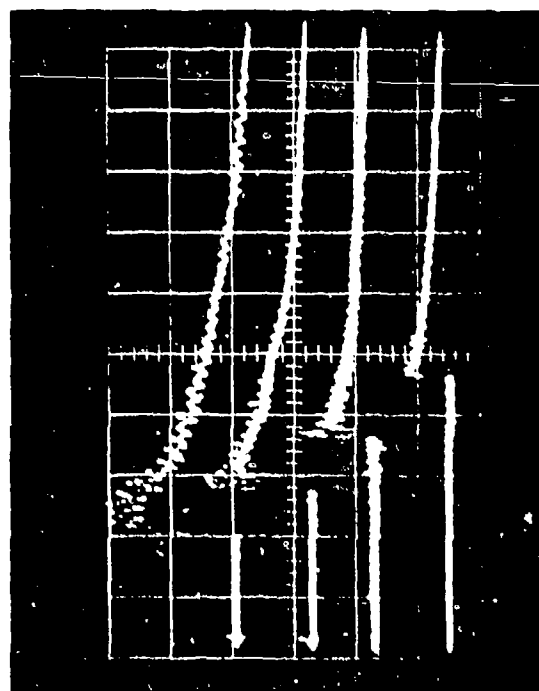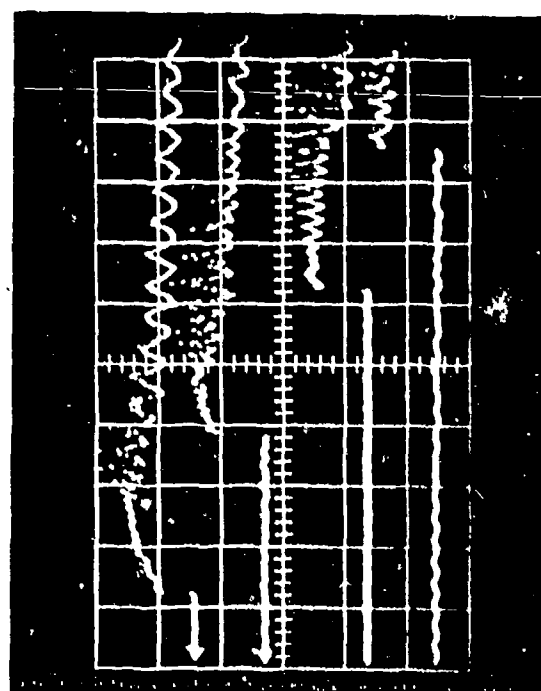Fig. 4

Fig. 5a

Fig. 6a

Fig. 8b

Fig. 8d
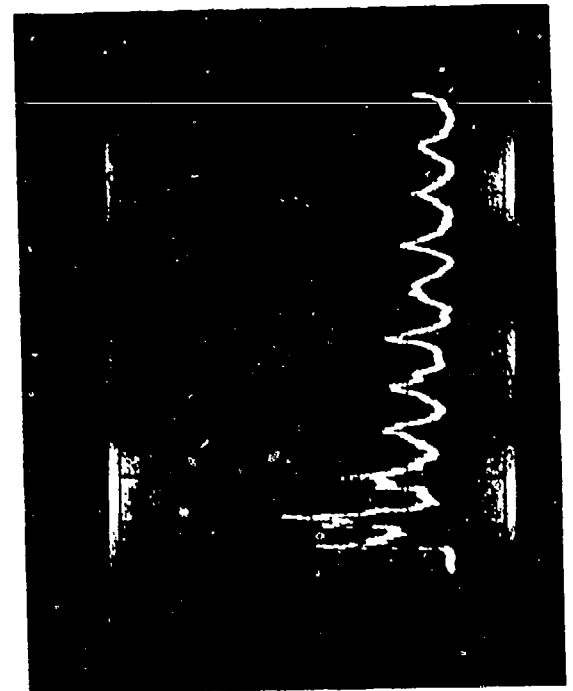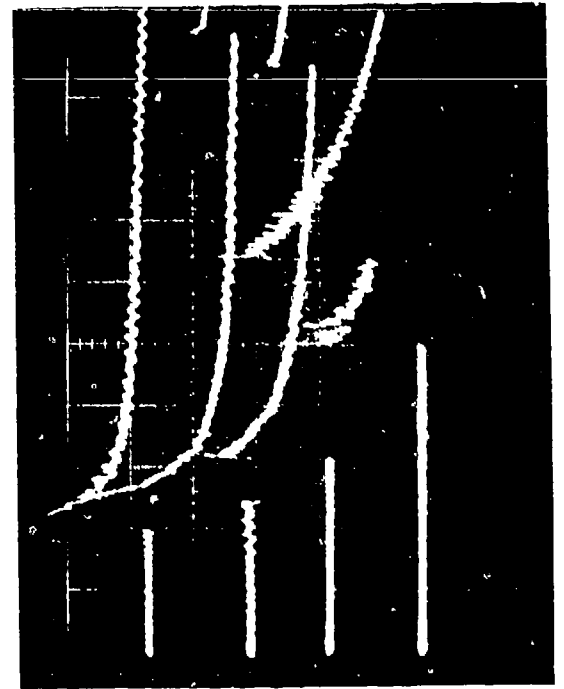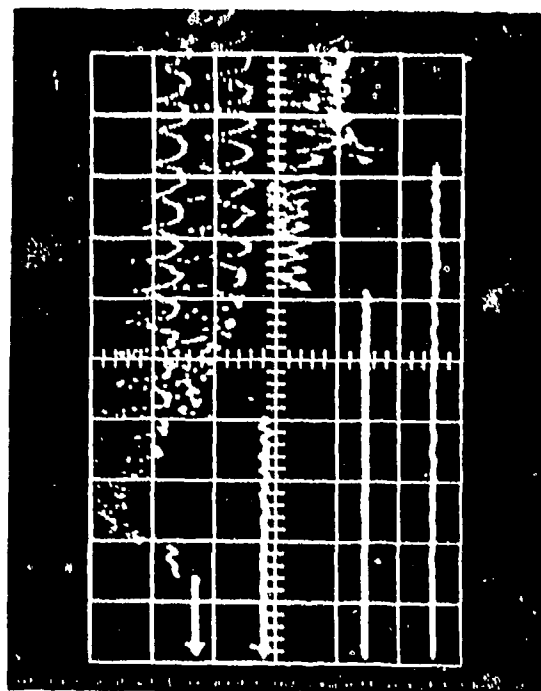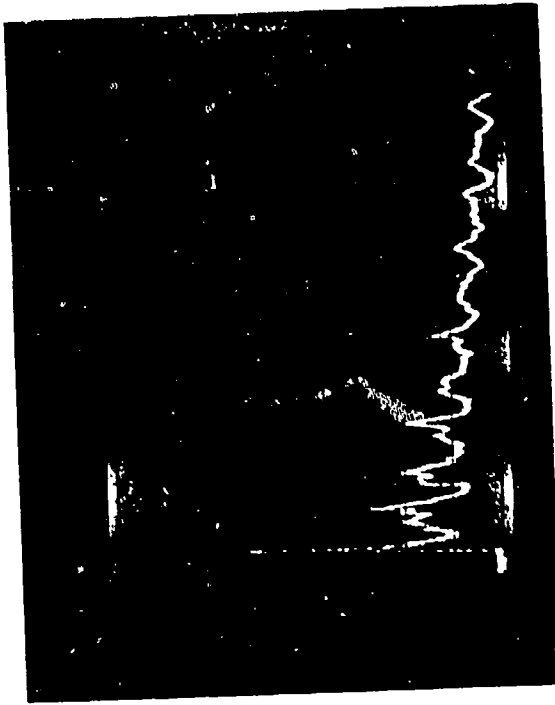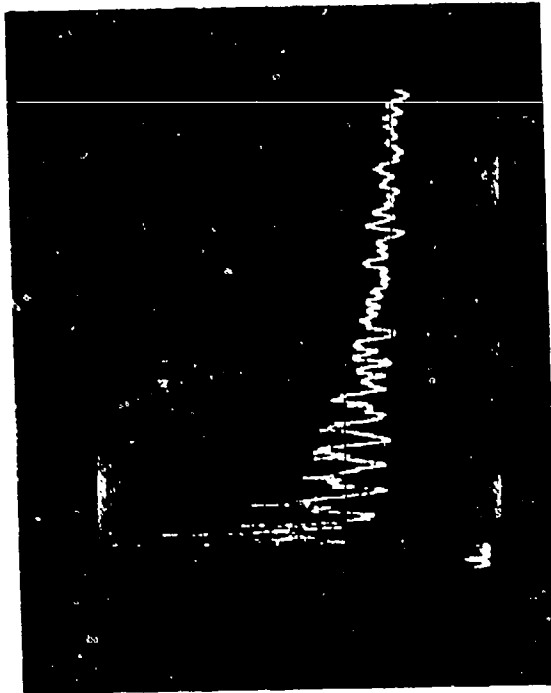
Fig. 8a
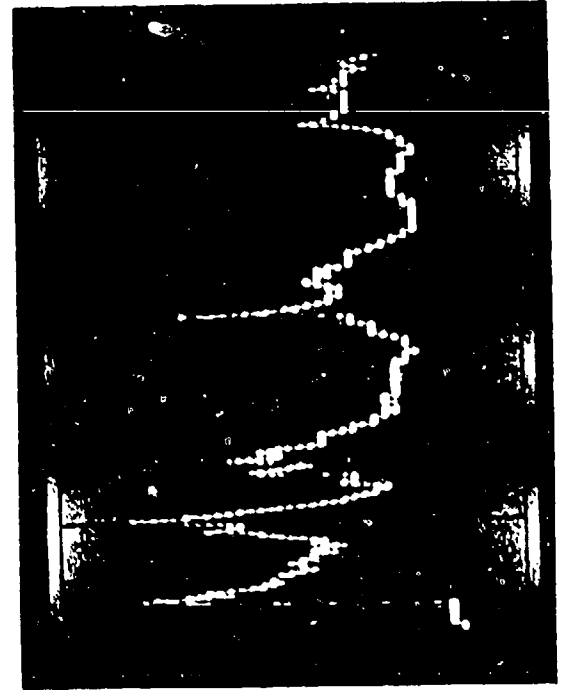
Fig. 8c

APPENDIX IV

On the Scaling of Blast Waves from Fuel-Air Explosives*

In a conventional, non-nuclear weapon, a strong blast wave of high energy density is generated by detonating in the surrounding atmosphere a concentrated charge of solid (or high) explosive (henceforth H.E.). Because of the relative small dimensions of the concentrated charge, the charge dimensions, its geometry and the characteristic time for the energy deposition can usually be ignored. Therefore, blast waves generated by concentrated charges approach ideal point blast behavior at relative close distances from the source. For these ideal explosions, nearly all the chemical energy released by the detonation process can be considered to be transferred to the shock front and subsequently dissipated in the surroundings as the blast wave propagates. Given the mass of the solid explosive charge, the blast energy E_o is thus known a priori for ideal explosions and a characteristic explosion length $R_o = (E_o/p_o)^{1/3}$ can be derived to scale all ideal explosions. The destructive potential of conventional weapons, i.e., the blast damages, can then be easily estimated from a standard chart giving point blast overpressures Δp_s and static and dynamic impulses I_s and I_d, respectively, with the scaled distance R_s/R_o where R_s denotes the shock radius[1].

For certain military applications, blast waves generated by fuel-air explosives (henceforth FAE) with moderate energy densities and moderate initial strengths may prove more effective. In an FAE weapon, the fuel is explosively disseminated in the atmosphere to form an explosive vapor cloud and then detonated subsequently by one or more initiating charges. Depending on the rate of fuel dispersion and the ignition delay, the vapor cloud dimensions (i.e., the cloud radius R_c) may be quite large. As a result of the relative large dimension of the cloud, vapor cloud explosions generate non-ideal blast waves which scale according to the cloud radius R_c in the near field. In the far field where the distances are large compared with the characteristic dimension of the cloud, FAE blast waves should decay according to the Bethe-Landau-Whitham asymptotic solution as in the case of ideal point blast waves, hence scale according to the explosion length R_o. There-

fore, FAE weapons require two characteristic lengths for scaling in the near and
far fields, respectively. Whereas the cloud radius R_c can readily be estimated,
the explosion length in FAE weapons can no longer be assessed a priori like in a
point blast explosion. For fuel-air explosives, the actual blast energy can no
longer be equated to the total combustion energy of the reactive mixture since a
significant portion remains in the combustion products in the form of internal
energy. Furthermore, because of the large dimensions of the FAE cloud, the blast
decay outside the cloud can be drastically affected by the details of the energy
release processes inside the cloud. In other words, the effective blast energy
may strongly depend on the various possible modes of combustion of the cloud (viz.,
detonation, volumetric explosion or deflagration). The effective energy should be
the actual work done by the expanding interface between the combustion products
and the surroundings. The blast energy cannot be assessed a priori since the path
of the interface and the pressure variation on the interface can only be determined
after solving for the blast flow structure itself. This in turn requires the nume-
rical integration of the gasdynamic equations with the appropriate initial and
boundary conditions of the problem. Such numerical computations are also very ex-
pensive because good accuracy in the far field requires the use of very fine step
sizes.

To estimate the blast energies from fuel-air and oxygen explosives, the
Authors[1] have used the simpler Brinkley-Kirkwood theory (henceforth B-K)[2] and match
the far field experimental overpressure decay with distance[3]. Good agreement was
achieved with blast energies representing approximately 20 and 25% of the heat re-
leased by detonative combustion in stoichiometric hydrocarbon-air and oxygen mix-
tures, respectively. On the other hand, Fishburn[4] using Oppenheim's numerical code
(viz., CLOUD code)[5] has estimated the blast energy from MAPP-air detonation at ap-
proximately 37.8% of the combustion energy. The CLOUD code does not calculate the
work done by the expanding interface, but the blast energy can be estimated from
the first law of thermodynamics and the interface position when the overpressure

at the interface returns to zero. Since MAPP-air detonation data[4] are very similar to the hydrocarbon-air data used in Ref. 1, it is difficult to explain the discrepancy in both estimates for fuel-air mixtures, the CLOUD code blast energy being almost twice as large as the value derived from the B-K theory.

Furthermore, blast energy estimates from volumetric explosions of MAPP-air and hydrocarbon-air mixtures differ only by a factor of 1.25. For MAPP-air, Fishburn's blast energy estimate of 33.6% of the combustion energy is almost equal to his blast energy estimate from detonation and suggests that blast energy may be independent of the combustion mode. For hydrocarbon-air volumetric explosion, the Authors[1] have estimated the blast energy at approximately 42% of the combustion energy by assuming an isentropic expansion of the explosion products since no experimental data were available to fit a curve of overpressure decay with distance as performed for the detonation case. This value which constitutes an upper bound for the work done by the expanding interface is more than twice the Author's blast energy estimate from detonation and suggests that blast energies in hydrocarbon-air mixtures depend on the mode of combustion in complete disagreement with Fishburn's conclusion. On the other hand, the Authors' blast energy estimate from volumetric explosion in hydrocarbon-oxygen mixtures of 22% of the combustion energy[1] compares well with their 25% estimate from detonation and tends to support Fishburn's conclusion regarding the independence of the blast energy from the mode of combustion in the cloud.

This is an important question to resolve since volumetric explosion may occur if partial or total confinement of the cloud is achieved or by heating uniformly the cloud to its auto-ignition limit by radiation or shock wave. The initial strength of the blast wave from volumetric explosion being approximately half the value from detonation results in a slower decay of the blast strength, hence, larger damages in the intermediate field[4]. Therefore, FAE weapons in which the explosive vapor cloud is volumetrically exploded may be quite attractive for military applications.

Reliable blast energy estimates from FAE should also resolve the important problem of far field equivalency. Far field equivalency implies that ideal blast waves from H.E. and non-dical blast waves from FAE are equivalent in the far field. In other words, on the basis of the blast energy alone, blast overpressure and impulses can be estimated for these explosions in the weak shock far field regime.

In this paper, a reliable numerical code is developed to compute the blast energy from vapor cloud explosions for far field scaling of non-ideal blast waves in relation with FAE weapons. The present study also resolves the important questions of blast energy dependence on the mode of combustion in the cloud and far field equivalency of H.E. and FAE blast waves using as a particular example the blast waves generated by centrally ignited detonations and volumetric explosions of spherical clouds of stoichiometric hydrocarbon-air and oxygen mixtures.

2. Vapor Cloud Explosion Models

2.i. C-J Detonation

Assume that at time $t = 0$, a C-J detonation is initiated at the center $r = 0$ of a reactive cloud of radius R_c and propagates at a constant velocity D in the reactive mixture. The burnt gases behind the C-J front are expanded and decelerated to zero velocity by a centered expansion wave. The self-similar flow field behind the C-J front can easily be computed for any given reactive mixture with prescribed initial conditions, namely, composition, pressure, temperature, specific heat ratios of unburnt and burnt gases and combustion energy[6].

When the detonation front reaches the cloud edge ($r = R_c$), a shock wave is transmitted into the surrounding atmosphere and an expansion wave propagates back into the explosion products. The subsequent flow structure inside and outside the cloud is no longer self-similar and can only be described by solving numerically the time-dependent, one-dimensional, spherically symmetric, adiabatic

equations for compressible, non-viscous and non-heating conducting, perfect gases subjected to appropriate boundary conditions, viz.,

$$\frac{\partial F}{\partial t} + \frac{\partial g}{\partial r} + S = 0 \tag{1}$$

where

$$F = \begin{bmatrix} \rho \\ \rho u \\ \rho e \end{bmatrix}, \quad g = \begin{bmatrix} \rho u \\ \rho u^2 + p \\ \rho u(e + p/\rho) \end{bmatrix}, \tag{2}$$

$$S = \begin{bmatrix} 2\rho u/r \\ 2\rho u^2/r \\ 2\rho u(e + p/\rho)/r \end{bmatrix}$$

$$e = p/(\gamma-1)\rho + u^2/2 \tag{3}$$

$$p = \rho RT \tag{4}$$

where ρ, p, T, u and γ denote the density, pressure, temperature, particle velocity and specific heat ratio, respectively. The relevant boundary conditions at the shock front are given by the Rankine-Hugoniot relations,

$$\rho(R_s,t)/\rho_0 = (\gamma_0+1)/(\gamma_0-1+2\eta)$$

$$u(R_s,t)/\dot{R}_s = 2(1-\eta)/(\gamma_0+1) \tag{5}$$

$$p(R_s,t)/\rho_0\dot{R}_s^2 = 2\left(1-(\gamma_0-1)\eta/2\gamma_0\right)/(\gamma_0+1)$$

where $\eta = M_s^{-2}$, M_s denotes the shock Mach number and subscripts s and o character-
ize the shock front and the initial conditions in the surrounding atmosphere. At
the center, the boundary conditions require the flow to be at rest, i.e.,

$$u(o,t) = 0 \quad , \quad t \geqslant 0 \tag{6}$$

2.ii. Volumetric Explosion

Assume at time t = 0, a volumetric explosion occurs in a reactive cloud
of radius R_c of prescribed composition and initial conditions as in 2.i. The re-
sulting pressure and temperature increases can easily be calculated by combining
the steady-state, conservation of mass, momentum and energy equations, viz.,

$$p_b/p_u = T_b/T_u = (\gamma_b - 1)(1/(\gamma_u - 1) + \gamma_u q) \tag{7}$$

where

$$q = \rho_u Q / \gamma_u p_u \tag{8}$$

Subscripts u and b characterize unburnt and burnt gases, respectively and Q denotes
the combustion energy per unit mass of reactive mixture. In deriving Eq. (7) it
has been assumed that the molecular weights of unburnt and burnt gases are the
same.

The subsequent propagation of the transmitted shock in the surrounding
atmosphere and the reflected expansion wave in the explosion products are obtained
by solving numerically the unsteady gasdynamic equations (Eqs. 1-6).

3. Numerical Analysis

The CLOUD code which solves the unsteady gasdynamic equations in

Lagrangian coordinates is very adequate to calculate the interface trajectory and properties to estimate the blast energy from vapor cloud explosions. However, the code which uses the von Neumann-Richtmeyer artificial viscosity to avoid shock discontinuities broadens the shock front and also creates numerical overshoots and undershoots which must be removed by the use of appropriate smoothing techniques.

The present numerical codes uses an Eulerian, finite-difference algorithm which combines Van Leer's first-order scheme[7] with Boris et al's flux corrected transport (FCT) technique[8-10] to handle accurately steep gradients associated with shock propagation and prevents large numerical overshoots or undershoots.

In Van Leer's first-order scheme, the centered difference scheme of Eq. (1) is stabilized by a diffusion term, viz.,

$$F_n(t + \Delta t) = F_n(t) + \Delta t \, \frac{\partial F_n}{\partial t}(t + \Delta t)$$

$$+ \frac{1}{2} k_{n+\frac{1}{2}}(t) \left[F_{n+1}(t) - F_n(t) \right] \qquad (9)$$

$$- \frac{1}{2} k_{n-\frac{1}{2}}(t) \left[F_n(t) - F_{n-1}(t) \right]$$

where the diffusion coefficients k are defined as

$$k_{n \pm \frac{1}{2}}(t) = \frac{1}{2} \left[k_n(t) + k_{n \pm 1}(t) \right] \qquad (10)$$

and

$$k_m(t) = \left[C_n(t) + |u_n(t)| \right]^2 (\Delta t/\Delta r)^2 \qquad (11)$$

where c_n and u_n are the local sound speed and particle velocity at the grid point n, respectively. To prevent overshoots near sharp gradients the time step Δt is restricted by the Courant-Friedrich-Lewy stability criterion

$$\Delta t = \sigma \Delta r_m / (C_n + |u_n|) \qquad (12)$$

where the Courant number σ is less than unity.

The FCT technique consists of three finite-difference operations: a transport and a diffusion followed by an antidiffusion. In the FCT technique, the value of the vector F in Eq. (1) is calculated at any grid point n at time $t + \Delta t$ in four steps. In the first step where transport and diffusion operations are performed, an approximate value for F_n at time $t + \Delta t$ is calculated by a finite-difference approximation to Eq. (1) at time $t + \Delta t/2$ and an additional diffusion term, viz.,

$$\widetilde{F}_m(t + \Delta t) = F_m(t) + \Delta t \frac{\partial F_m}{\partial t}(t + \Delta t/2)$$

$$+ \nu_{m+\frac{1}{2}} \left[F_{m+1}(t) - F_m(t) \right] \qquad (13)$$

$$- \nu_{m-\frac{1}{2}} \left[F_m(t) - F_{m-1}(t) \right]$$

The diffusion term added in Eq. (13) is an error with respect to Eq. (1) and is removed in the fourth step by adding an equal but opposite antidiffusion

in Eq. (13).

Some provisional fluxes necessary to remove the three-point diffusive error term are calculated in the second step, viz.,

$$\tilde{\phi}_{n+\frac{1}{2}}(t+\Delta t) = \nu_{n+\frac{1}{2}}\left[\tilde{F}_{n+1}(t+\Delta t) - \tilde{F}_{n}(t+\Delta t)\right] \quad (14)$$

These fluxes are then corrected in the third step to prevent the formation of new extrema in the solution or the amplification of existing extrema when used to perform in the fourth step the antidiffusion of the first step. The antidiffusion fluxes are given by

$$\phi_{n+\frac{1}{2}}(t+\Delta t) = sgn\,\tilde{\Delta}_{n+\frac{1}{2}} \cdot max\left[\,0,\right.$$

$$(15)$$

$$\left. min\left\{\tilde{\Delta}_{n-\frac{1}{2}}\,sgn\,\tilde{\Delta}_{n+\frac{1}{2}}, |\tilde{\phi}_{n+\frac{1}{2}}|, \tilde{\Delta}_{n+\frac{3}{2}}\,sgn\,\tilde{\Delta}_{n+\frac{1}{2}}\right\}\right]$$

where

$$\tilde{\Delta}_{n+\frac{1}{2}} = \tilde{F}_{n+1}(t+\Delta t) - \tilde{F}_{n}(t+\Delta t)$$

In the last step, antidiffusion is performed to obtain the value of the vector F at time t + Δt, viz.,

$$F_{n}(t+\Delta t) = \tilde{F}_{n}(t+\Delta t) - \phi_{n+\frac{1}{2}}(t+\Delta t)$$

$$(16)$$

$$+ \phi_{n-\frac{1}{2}}(t+\Delta t)$$

This technique which prevents the formation of extrema associated with

the diffusion term does not remove valid physical extrema arising from the term $\partial F/\partial t$ in Eq. (1).

Combining Van Leer's scheme with the FCT technique, i.e., substituting for Eq. (13), the first step in FCT, the following transport and diffusion operations,

$$\tilde{F}_n(t+\Delta t) = F_n(t) + \Delta t \frac{\partial F_n}{\partial t}(t+\Delta t)$$

$$+ \left(\frac{1}{2}k_{n+\frac{1}{2}}(t) + D_{n+\frac{1}{2}}\right)\left[F_{n+1}(t) - F_n(t)\right] \tag{17}$$

$$- \left(\frac{1}{2}k_{n-\frac{1}{2}}(t) + D_{n-\frac{1}{2}}\right)\left[F_n(t) - F_{n-1}(t)\right]$$

yields less expensive, more accurate and stable solutions to some gasdynamic problems than by applying each method separately. Therefore, the Van Leer-FCT numerical method has been used to compute the flow structure associated with vapor cloud explosions.

4. Results and Discussion

The propagation in air of non-ideal blast waves generated by centrally initiated detonation and/or volumetric explosion of spherical clouds of stoichiometric propane-air and oxygen mixtures at initial pressure and temperature of 1 atmosphere and $25^{\circ}C$, respectively, have been computed numerically using the Eulerian code described in Section 3. Propane was chosen as the fuel because it represents a typical hydrocarbon and furthermore experimental blast data exist for meaningful comparison. For both mixtures, the relevant properties corresponding to both combustion modes are given in Table 1. Because of the differences in the

specific heat ratios of the combustion products and air, the specific heat ratio was varied smoothly around the interface from the explosion product value to the air value to prevent the formation of overshoots around the interface. The interface location was obtained from mass conservation of the explosion products, viz.,

$$\int_0^{R_i(t)} 4\pi r^2 \rho \, dr = \frac{4\pi}{3} R_c^3 \rho_u$$

where R_i denotes the instantaneous location of the interface and subscript u characterizes the unburnt mixture. The pressure at the interface was calculated by linear interpolation. Numerical calculations were carried out to blast overpressures of approximately 0.1 atmosphere and the FCT diffusion coefficient ν was kept constant at a value of 1/8.

Typical pressure profiles for a propane-air detonation and volumetric explosion, plotted in Figs. 1 and 2 with respect to distance scaled according to the cloud radius R_c, demonstrate the stability of the numerical technique and its ability to handle sharp discontinuities. Similar profiles were obtained for propane-oxygen mixtures with faster decay rates associated with higher initial blast overpressures.

Blast energies defined as the work done by the expanding interface prior to the formation of the negative overpressure phase are found to represent approximately 36, 34 and 27% of the combustion energies of detonated propane-air, ethylene-air and propane-oxygen mixtures, respectively. The propane-oxygen value compares well with the Author's previous estimate of 25% of the combustion energy[1]. On the other hand, the present fuel-air data which compares well with Fishburn's value for MAPP[4] of 37.8%, completely disagrees with our previous estimate of almost 20[1] and demonstrates the danger of using fitting techniques.

For volumetric explosions of propane-air and oxygen mixtures, the blast energies represent approximately 34 and 27% of the respective combustion energies

of these mixtures and differ from the corresponding blast energies from detonation by 6 and 1%, respectively. Therefore, the present results support and extend Fishburn's conclusion that blast energies from fuel-air and oxygen mixtures are almost independent of the mode of combustion of the explosive cloud (i.e., detonation or volumetric explosion). The larger percentage of combustion energy appearing as blast energy for fuel-air explosions reflects the smallest entropy increase associated with fuel-air combustion (approximately 60% less than for fuel-oxygen mixtures). Assuming an isentropic expansion of the combustion products to ambient pressure, the percentages of combustion energy remaining in the combustion products as internal energy have been estimated at about 57 and 70% for fuel-air and oxygen mixtures, respectively, in good agreement with the corresponding blast energies.

Non-ideal blast wave overpressures and impulses generated by fuel-air and oxygen explosions plotted in Fig. 3 show far field equivalency when scaled with respect to the explosion length R_o. The B-K theory was used to generate the far field data. Starting at 5 cloud radii, the B-K data were found in excellent agreement with the numerical data which were computed down to about 10 cloud radii, except for the propane-oxygen static impulses. The B-K results for this parameter are 20% smaller than the numerical results and may reflect the breakdown of the B-K assumption for impulse for fuel-oxygen mixtures.

In the near-field, blast parameters reflect the non-idealities of the explosion, namely the mode of combustion and the nature of the oxidizer. Volumetric explosions are seen to be more destructive in the intermediate field where the blast wave decay is slower than the decay resulting from detonation of the vapor cloud.

Ideal point blast parameters also plotted in Fig. 3 decay faster than the non-ideal data in the intermediate and far fields. In other words, strong blast waves of high energy density generated by solid explosives are less destructive in the intermediate and far fields than the moderate strength blast waves

associated with smaller energy density explosions. By matching the far field behavior, an equivalent blast energy ratio E_q can be obtained. In the present study, the the overpressure curves have been matched at 0.01 atmosphere where the corresponding scaled distances R/R_o are 1.7 and 2.4 for ideal and non-ideal blast waves, respectively. The equivalent blast energy ratio E_q is $(1.7/2.4)^3 = 2.8$. Therefore, the destructive potential of a non-ideal blast wave from fuel-air or oxygen detonation or volumetric explosion is equivalent to that of an ideal point blast explosion with nearly three times the explosion energy. This is a consequence of the larger dissipation of energy in point blast with high initial overpressure. By the time the point blast wave has decayed to an acoustic wave, almost no energy is left in the N-wave. In contrast, non-ideal blast waves of moderate initial overpressure dissipate less energy as they propagate, hence still retain in the far-field a significant portion of their energy.

Using the effective blast wave energy for scaling non-ideal blast waves, theoretical blast parameters are compared in Fig. 4 with experimental data[3]. The latter were obtained in spherical balloons of diameters ranging from 0.7 to 6 meters, centrally ignited. The data are representative of detonations in several hydrocarbon-air and oxygen mixtures and show no dependence on the fuel and a slight dependence on the nature of the oxidizer (air or pure oxygen). Empirical formulae derived in Ref. 3 to fit the experimental data have also been plotted in Fig. 4. The measurements were carried out to distances of 50 cloud radii. Theoretical overpressures in the far field differ from the experimental data at most by 10%, well within the 5-10% accuracy of the measurements. The corresponding static impulses show less agreement (20% greater than the experimental data) in view of the difficulties associated with static impulse measurements.

5. Conclusions

A Eulerian numerical code using a flux-corrected transport technique capable of handling accurately sharp discontinuities like shock waves has been

developed to compute the effective energy of non-ideal blast waves generated by FAE weapons. For most hydrocarbon-air mixtures, it is found that almost 37% of the combustion energy actually goes to the blast wave and this fraction decreases for mixtures with higher energy densities (eg., about 27% for fuel-oxygen mixtures). Furthermore, the effective blast energy of fuel-air and oxygen mixtures exhibit no significant dependence on the mode of combustion of the reactive mixture whether detonation or volumetric explosion. On the basis of the effective blast energy, non-ideal blast waves from fuel-air and oxygen explosives are all equivalent in the far field and the blast parameters (eg., overpressure, static and dynamic impulses) scale according to the explosion length. However, far field equivalence for ideal and non-ideal blast waves does not exist. In other words, far field blast parameters from ideal and non-ideal explosions are not equal at the same scaled distance. By matching the blast overpressure curves in the far field, the equivalent point source energy for the non-ideal blast wave from a fuel-air or oxygen explosive weapon is three times greater than the energy from a point blast. As a result, the destructive potential of non-ideal blast waves from FAE weapons is found to be superior to that of conventional H.E. weapons in the far field.

References

1. J.H. Lee, C.M. Guirao, K.W. Chiu and G.G. Bach, "Blast Effects from Vapor Cloud Explosions", AIChE Loss Prevention Symposium, Houston, Texas (1977); also, Loss Prevention, 11, 59 (1977).

2. S.R. Brinkley and J.G. Kirkwood, "Theory of the Propagation of Shock Waves", Physical Review, 71, 9, 606 (1947).

3. S.M. Kogarko, V.V. Adushkin and A.G. Lvamin, "An Investigation of Spherical Detonations of Gas Mixtures", International Chemical Engineering, 6, 3 (1966).

4. B.D. Fishburn, "Some Aspects from Fuel-Air Explosives", Acta stronautica, 4, 375 (1977).

5. L.M. Cohen, J.M. Short and A.K. Oppenheim, "A Computational Technique for the Evaluation of Dynamic Effects of Exothermic Reactions", Combustion and Flame, 24, 319 (1975).

6. J.H. Lee, R. Knvstautis and G.G. Bach, "Theory of Explosions", AFOSR Scientific Report, AFOSR 69-3090 TR (1969).

7. B. Van Leer, "Stabilization of Difference Schemes for the Equations of Inviscid Compressible Flow by Artificial Diffusion", Journal of Computational Physics, 3, 473 (1969).

8. J.P. Boris and D.L. Book, "Flux Corrected Transport. I. SHASTA, A Fluid Transport Algorithm that Works", Journal of Computational Physics, 11, 38 (1973).

9. D.L. Book, J.P. Boris and K. Hain, "Flux-Corrected Transport. II: Generalization of the Method", Journal of Computational Physics, 18, 248 (1975).

10. J.P. Boris and D.L. Book, "Flux-Corrected Transport. III. Minimal-Error FCT Algorithms", Journal of Computational Physics, 20, 397 (1976).

Table 1

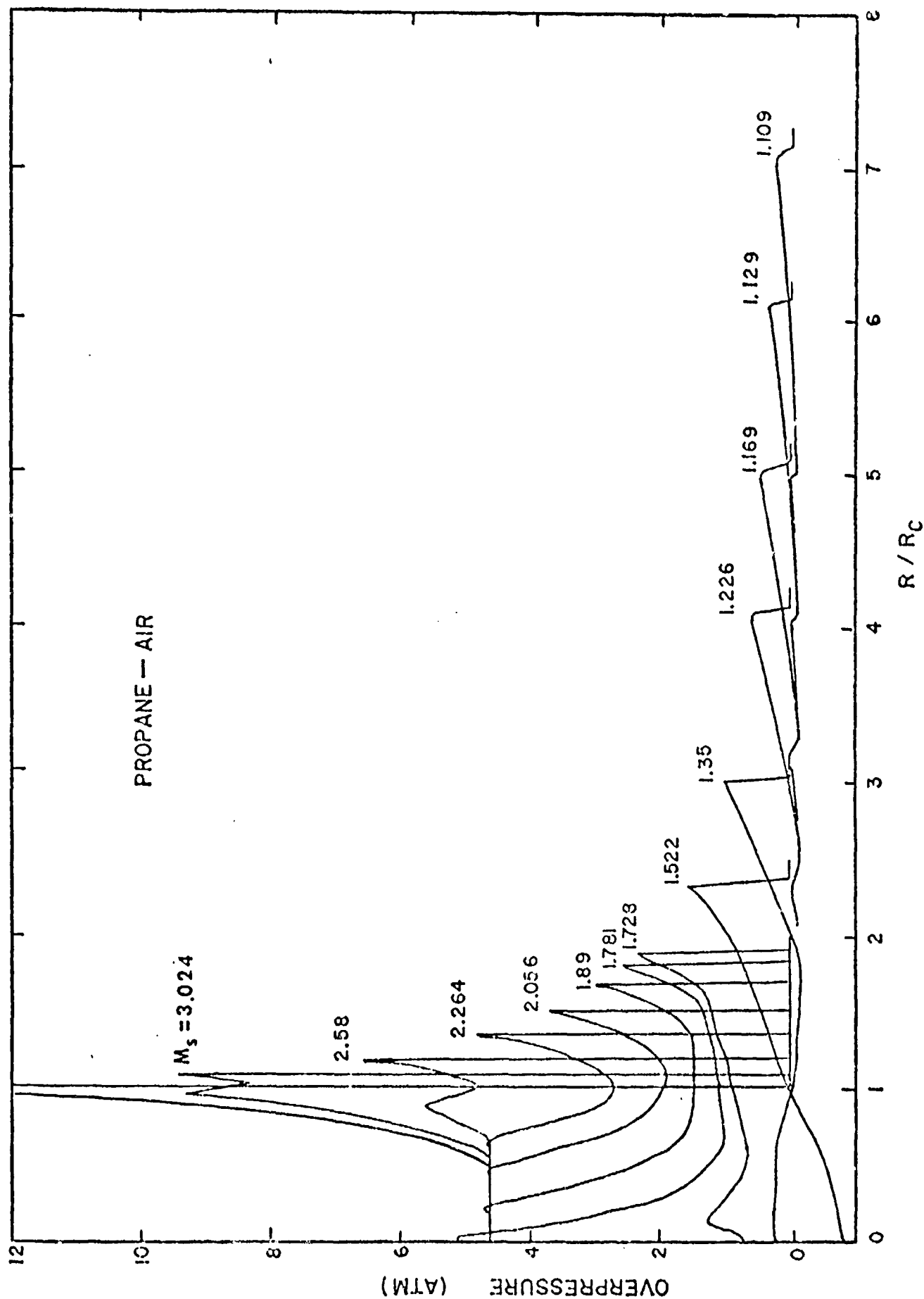| Mixture | Fuel, % | γ_u | Detonation | | Volumetric Explosion | | Q (kcal/kg) |
			Δp_d (atm)	γ_b	Δp_v (atm)	γ_b	
C_3H_8-Air	4.	1.37	17.27	1.28	8.34	1.26	668
C_2H_4-Air	6.53	1.38	17.74	1.27	8.32	1.25	720
C_3H_8-O_2	16.67	1.29	35.2	1.13	17.2	1.136	2400

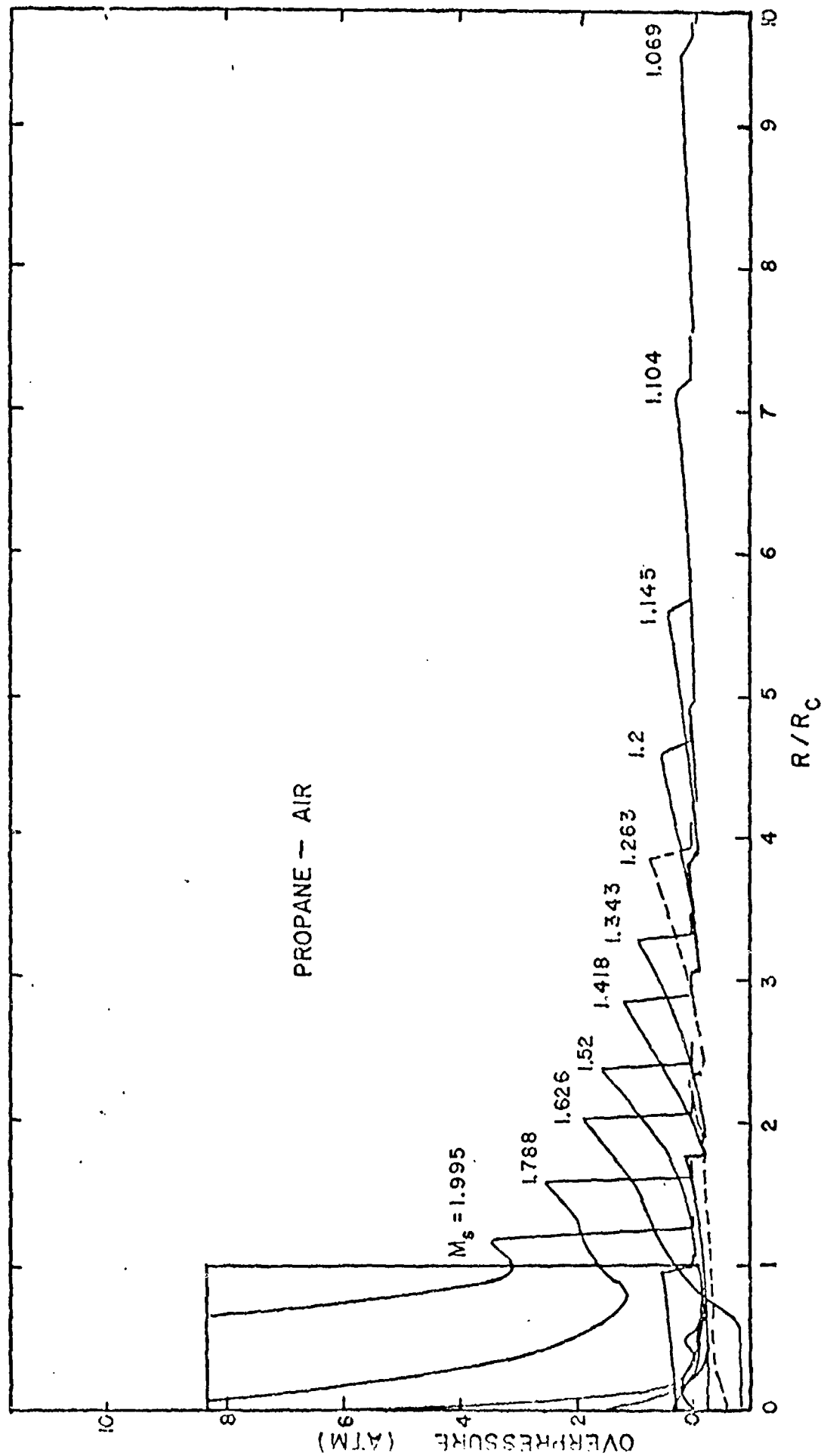Fig. 7   Pressure profiles from stoichiometric propane-air spherical detonation

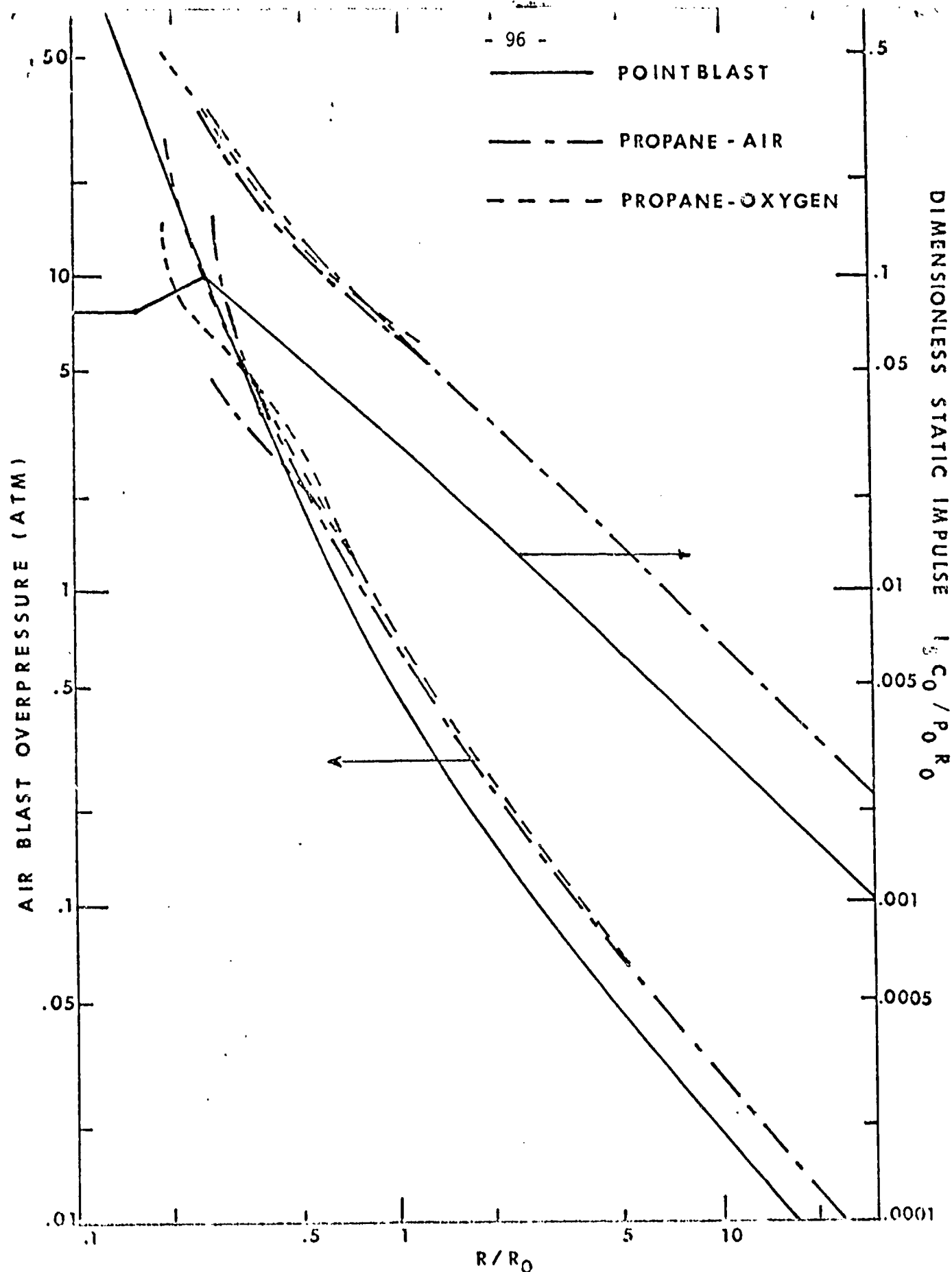Fig. 2   Pressure profiles from stoichiometric propane-air volumetric explosion.

Fig. 3   Air blast overpressure and static impulse decays with scaled distance
R/R_0 for ideal point blasts, spherical detonations and volumetric explosions
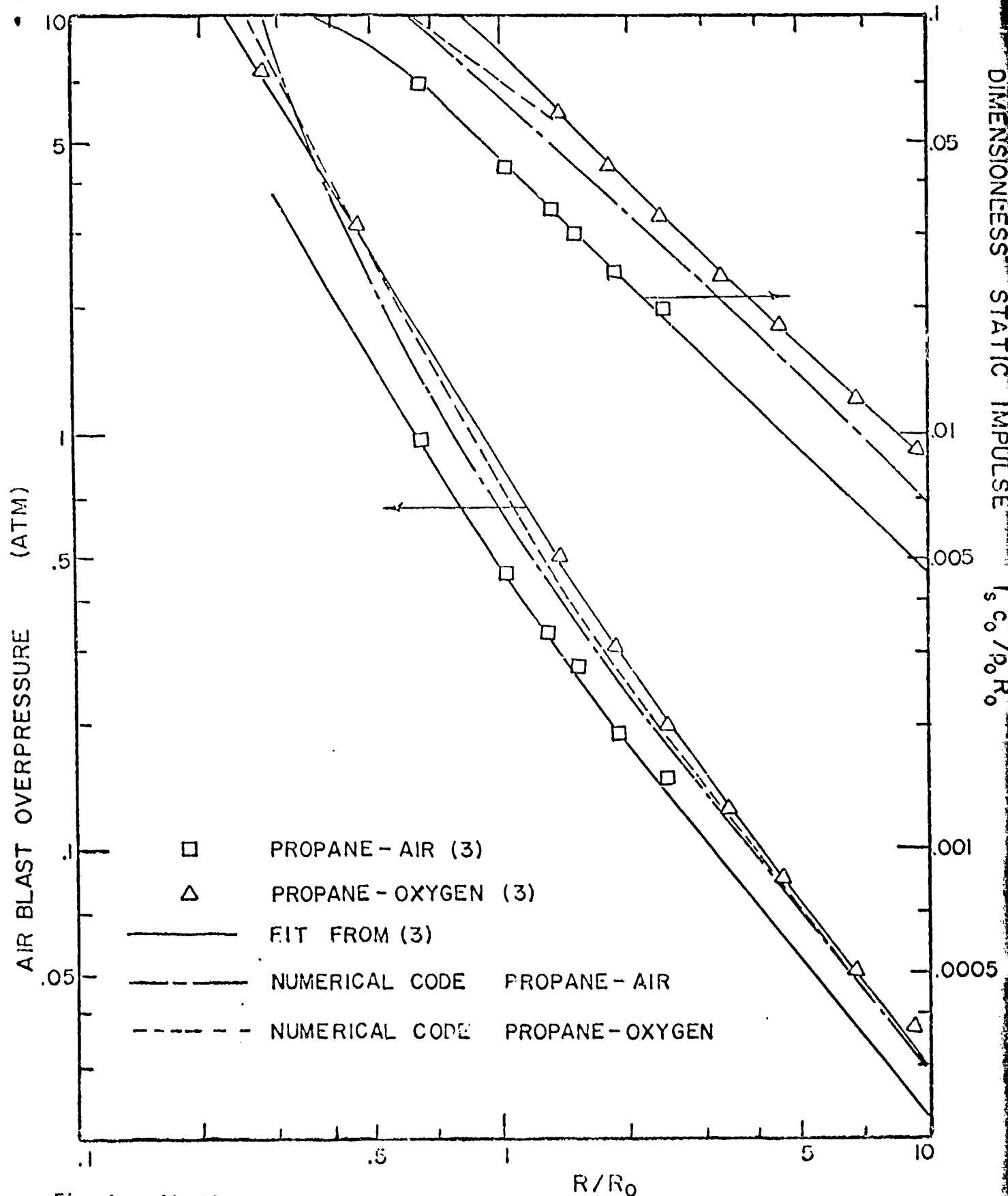in stoichiometric propane-air and oxygen mixtures.

Fig. 4   Air blast overpressure and static impulse decays with scaled distance R/R_c for spherical detonations in stoichiometric propane-air and oxygen mixtures